Electronic Supplementary Material (ESI) for Polymer Chemistry.

Supplementary Information

Metallosupramolecular Polymers as Precursors for Platinum Nanocomposites

Claudio Cappelletti,[1] Luis M. Olaechea,[1] Alessandro Ianiro,[1]

Cristina Prado-Martínez,[1] Emad Oveisi,[2] Christoph Weder,[1,] Stephen Schrettl[1,*]*

[1] Adolphe Merkle Institute, University of Fribourg
Chemin des Verdiers 4, 1700 Fribourg, Switzerland

[2] Interdisciplinary Centre for Electron Microscopy
EPFL, 1015 Lausanne, Switzerland

** To whom correspondence should be addressed:*

christoph.weder@unifr.ch

stephen.schrettl@unifr.ch

Table of Contents

1. Supplementary Figures S1–S31

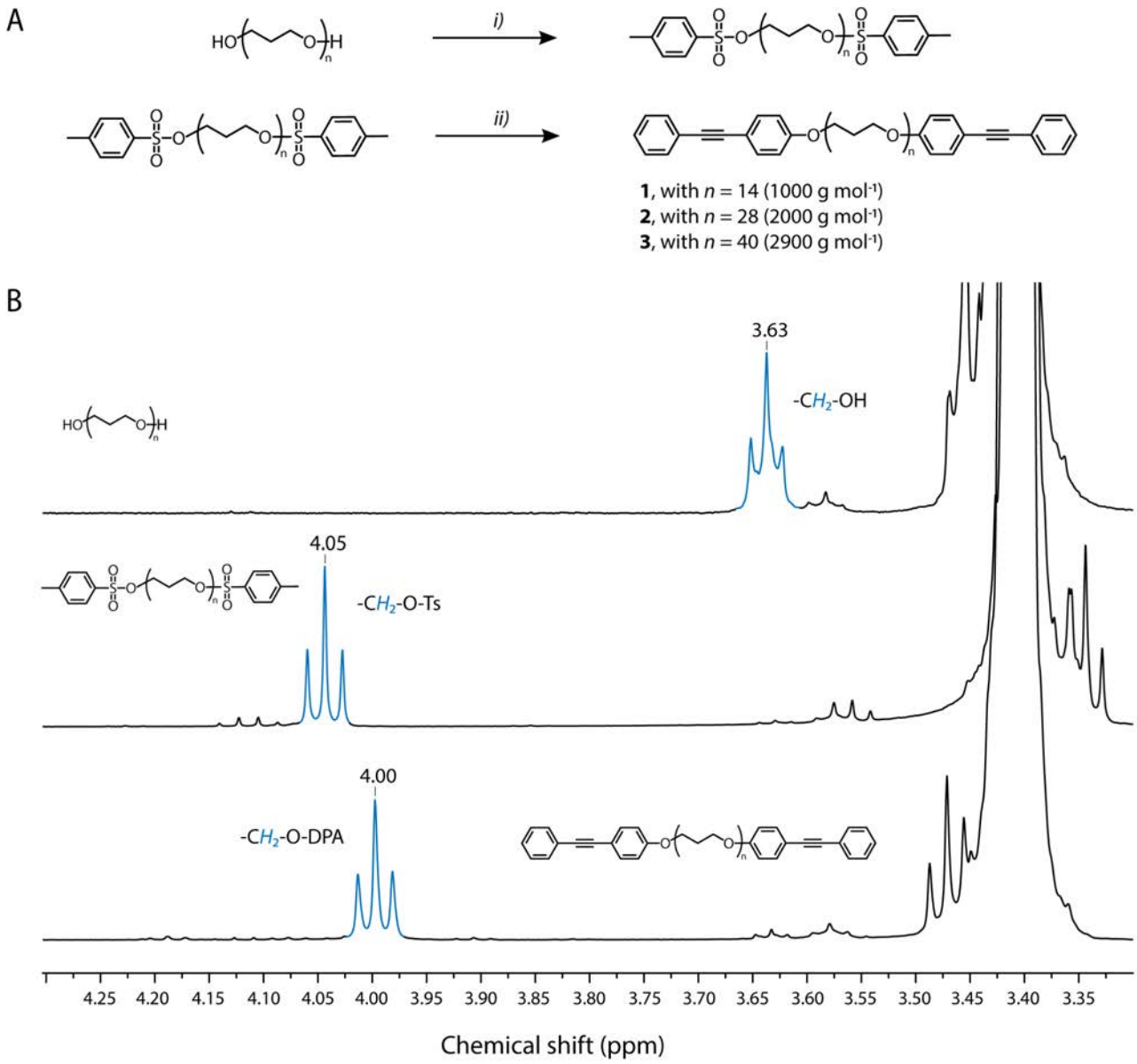

Supplementary Figure S1. (*a*) Schematic of the synthesis of the telechelic diphenylacetylene-functionalized poly(tetrahydrofuran) (PTHF) macromonomers **1**–**3** that were prepared from hydroxyl-terminated PTHF with a number-average molecular weight (M_n) of 1000, 2000, or 2900 g mol^{-1}. *Reagents and conditions: i) p*-toluenesulfonyl-chloride, pyridine, DCM, room temperature, 73%; *ii*) 4-(phenylethynyl)phenol, K_2CO_3, DMF/toluene (1:1), 100 °C, 78%. (*b*) Comparison of the sections of the ^{1}H NMR spectra (400 MHz, 297.2 K, $CDCl_3$) that show the signals associated with the methylene groups (–O–C*H*$_2$–) for the bis-hydroxyl-terminated PTHF (top), the bis-tosyl-terminated PTHF (center), and the bis-diphenylacetylene (DPA) terminated macromonomer **2** (bottom). The shift of the signals indicates full conversion (within the limits of ^{1}H-NMR spectroscopy).

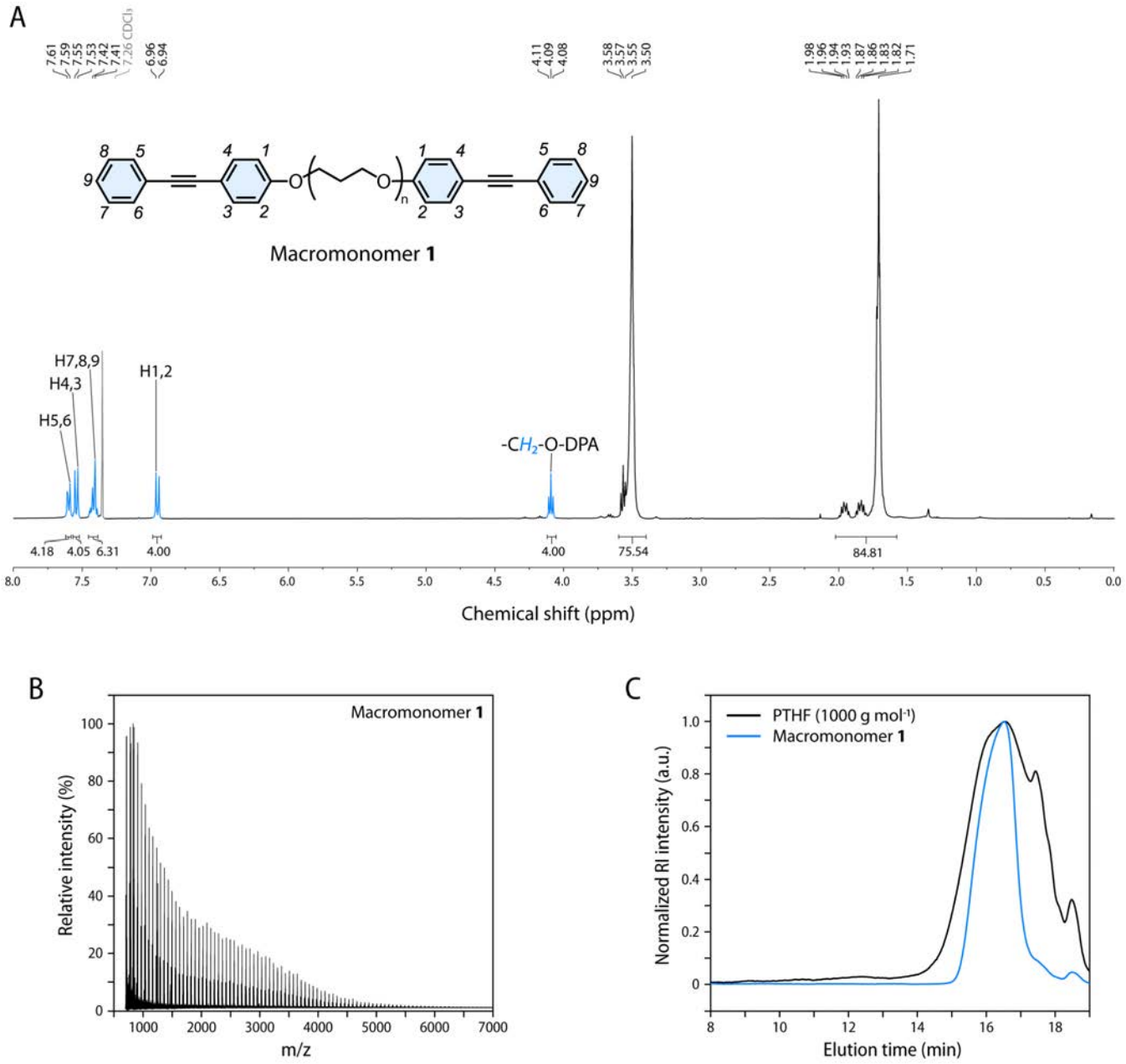

Supplementary Figure S2. (*a*) ^{1}H-NMR spectrum (400 MHz, 297.2 K, $CDCl_3$) of **1** (c = 0.001 mmol L^{-1}). (*b*) Matrix-assisted laser desorption/ionization (MALDI) time-of-flight (TOF) mass spectrum of macromonomer **1** (DCTB matrix). (*c*) Comparison of the size exclusion chromatography (SEC) traces of the hydroxyl-terminated poly(tetrahydrofuran) (1000 g mol^{-1}; black) and the macromonomer **1** (blue).

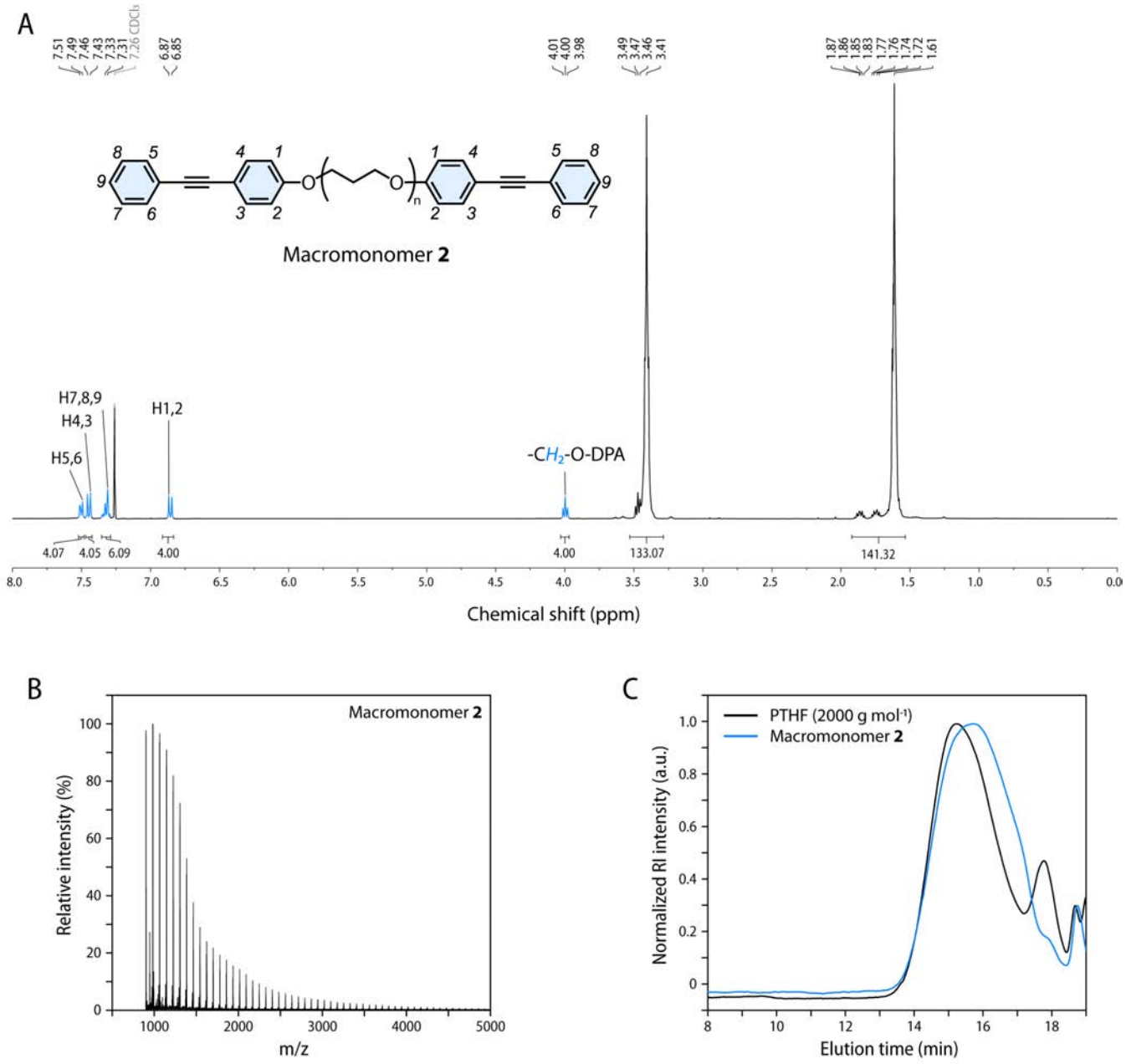

Supplementary Figure S3. (*a*) ^{1}H-NMR spectrum (400 MHz, 297.2 K, $CDCl_3$) of **2** (c = 0.001 mmol L^{-1}). (*b*) Matrix-assisted laser desorption/ionization (MALDI) time-of-flight (TOF) mass spectrum of macromonomer **2** (DCTB matrix). (*c*) Comparison of the size exclusion chromatography (SEC) traces of the hydroxyl-terminated poly(tetrahydrofuran) (2000 g mol^{-1}; black) and the macromonomer **2** (blue).

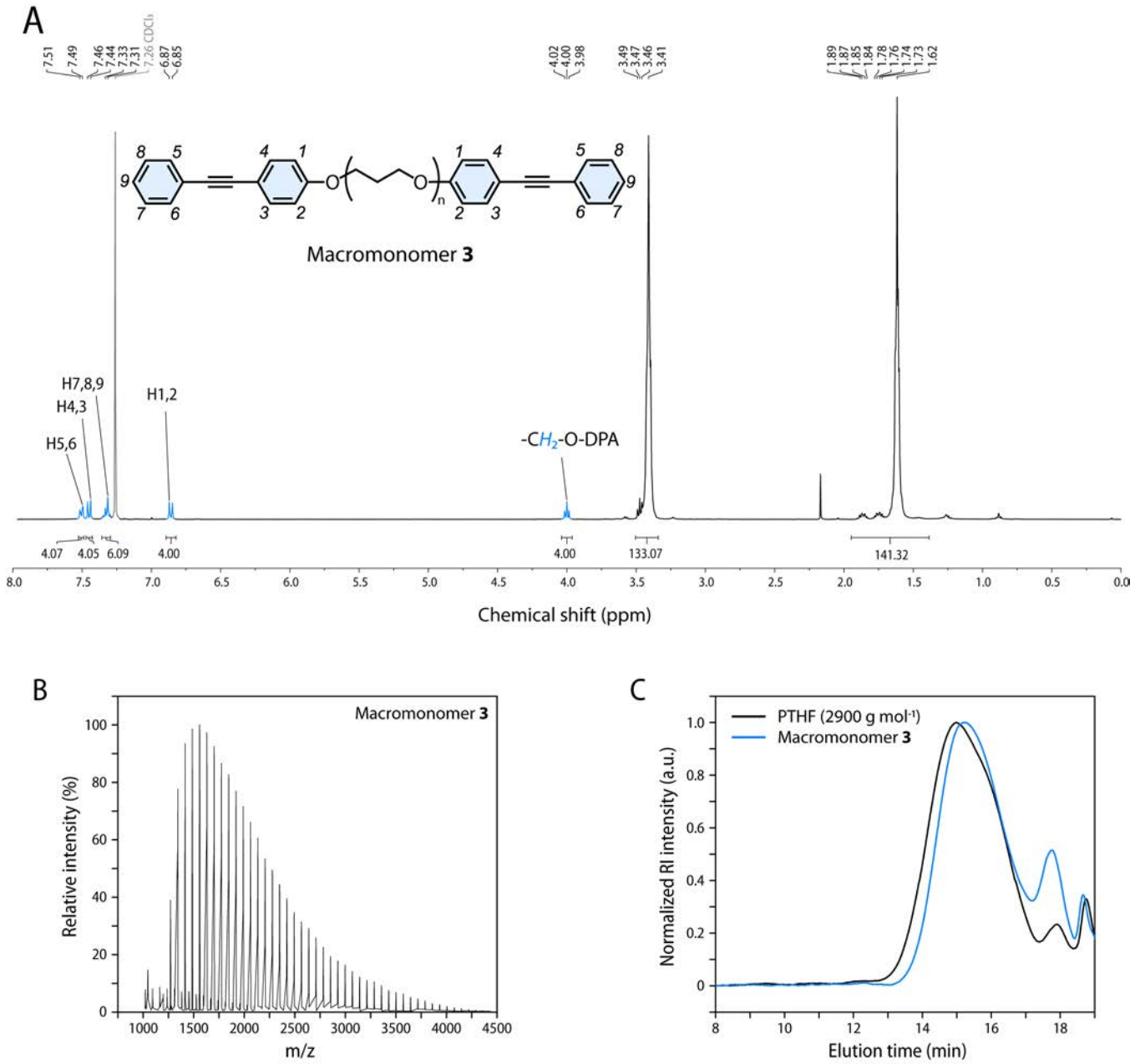

Supplementary Figure S4. (*a*) ^{1}H-NMR spectrum (400 MHz, 297.2 K, $CDCl_3$) of **3** (c = 0.001 mmol L^{-1}). (*b*) Matrix-assisted laser desorption/ionization (MALDI) time-of-flight (TOF) mass spectrum of macromonomer **3** (DCTB matrix). (*c*) Comparison of the size exclusion chromatography (SEC) traces of the hydroxyl-terminated poly(tetrahydrofuran) (1000 g mol^{-1}; black) and the macromonomer **3** (blue).

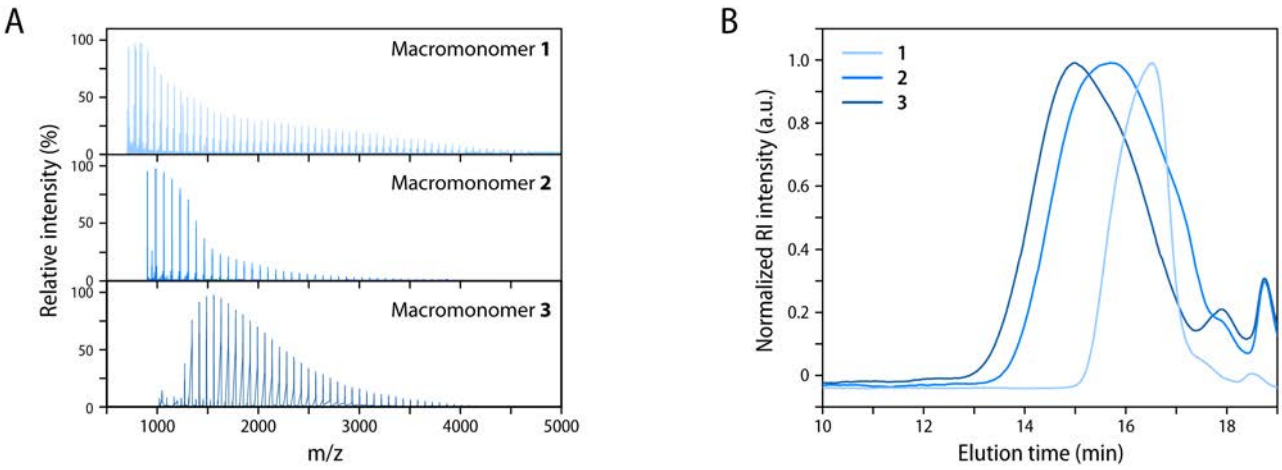

Supplementary Figure S5. Comparison of (*a*) the MALDI-TOF mass spectra (DCTB matrix) and (*b*) the SEC traces of the macromonomers **1–3**.

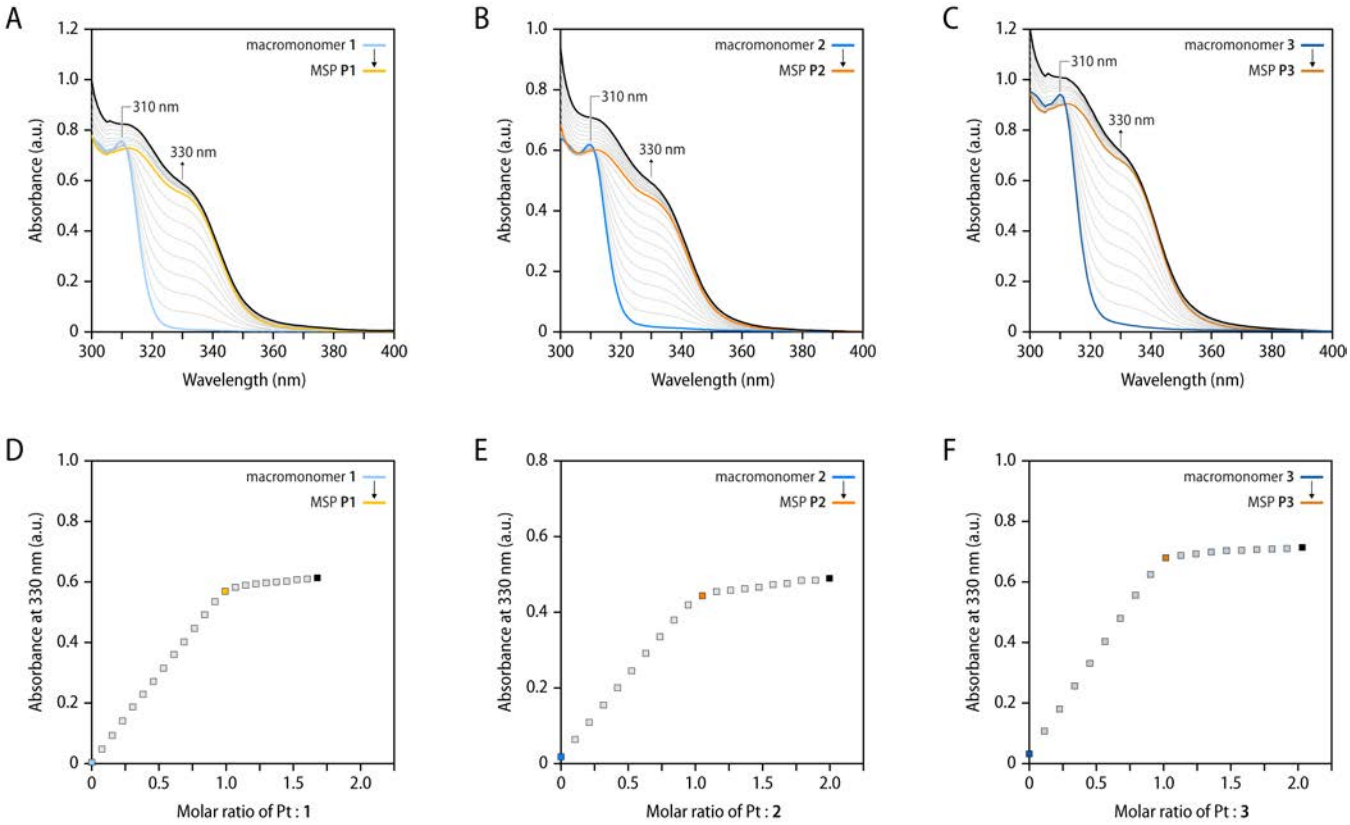

Supplementary Figure S6. Spectrophotometric titrations of the macromonomers **1**–**3** with aliquots of a $Pt^{(0)}(styrene)_3$ solution show the successful formation of the bis(η^2-alkyne)Pt^0 complexes at a 1:2 metal-to-ligand stoichiometry furnishing the metallosupramolecular polymers **P1**–**P3**. (*A*–*C*) UV-vis absorption spectra for (*a*) **1** (c = 12.6 μmol L^{-1}), (*b*) **2** (c = 10.9 μmol L^{-1}), and (*c*) **3** (c = 16.3 μmol L^{-1}) in $CHCl_3$ and upon addition of aliquots of $Pt^{(0)}(styrene)_3$ (c = 0.7, 0.8, and 1.1 mmol L^{-1}, respectively for each titration). The formation of the bis(η^2-alkyne)Pt^0 complexes is indicated by the increase in the intensity of the band at 330 nm. (*d*–*f*) Plots of the absorbance at λ_{max} = 330 nm and the molar ratio of Pt and (*d*) **1**, (*e*) **2,** and (*f*) **3** show that the bis(η^2-alkyne)Pt^0 complexes form at a 1:2 metal-to-ligand stoichiometry.

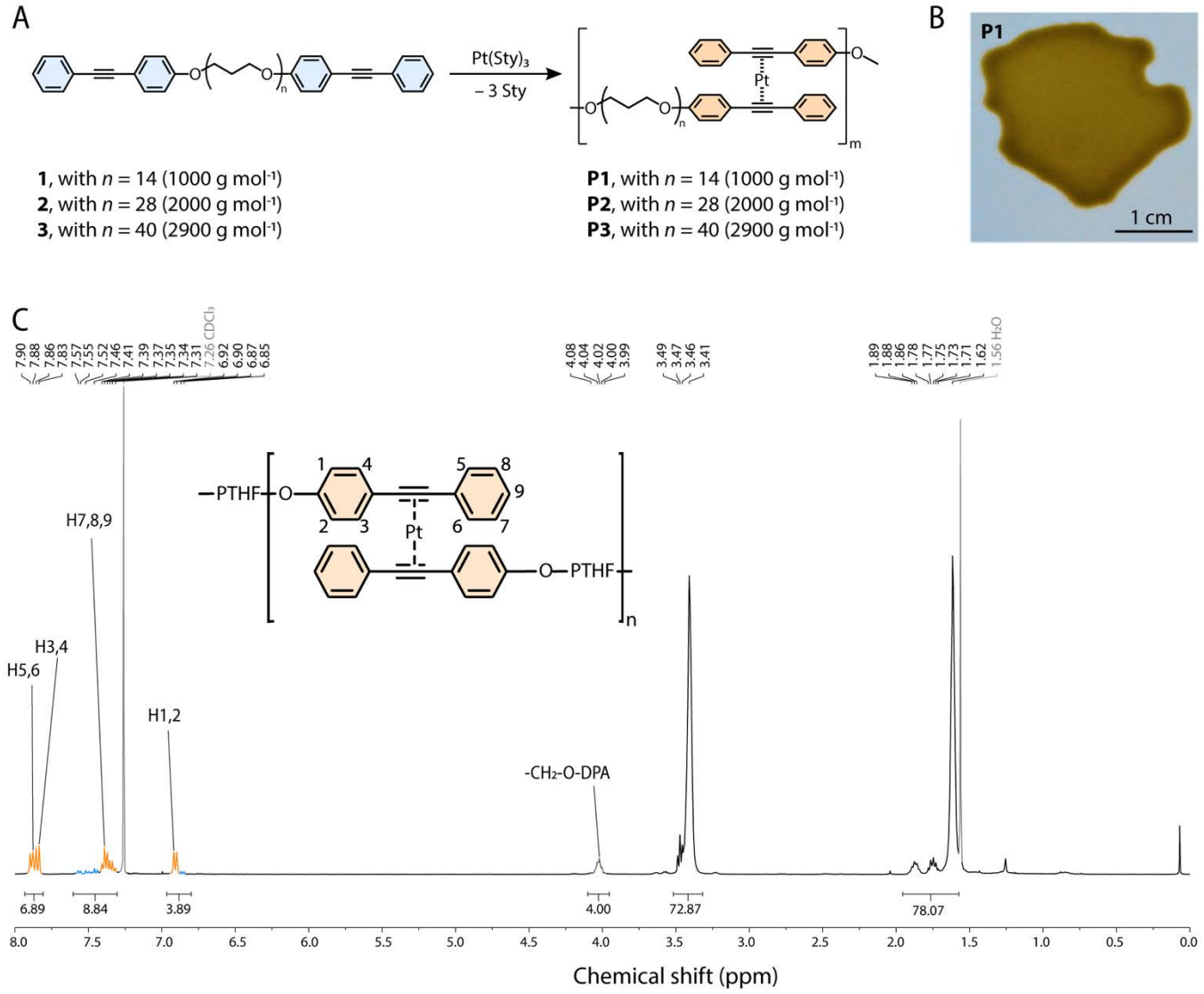

Supplementary Figure S7. (*a*) Scheme depicting the synthesis of the metallosupramolecular polymers **P1–P3** by the ligand exchange-driven polymerization of the telechelic diphenylacetylene-functionalized poly(tetrahydrofuran) macromonomers **1** ($n \approx 14$), **2** ($n \approx 28$), and **3** ($n \approx 40$) with Pt(styrene)$_3$. *Reagents and conditions:* Pt(styrene)$_3$ in styrene (c = 23 µmol L^{-1}), 1 h, room temperature. (*b*) Picture of a film of **P1** that was obtained by addition of stoichiometric quantities of Pt(styrene)$_3$ to a styrene solution of **1**. A 1:2 metal-to-ligand ratio was adjusted based on the spectrophotometric titrations and the mixture was solvent cast onto a glass substrate and left to dry for 24 h under ambient conditions. (*c*) ^{1}H-NMR spectrum (400 MHz, 297.2 K, $CDCl_3$) of **P1** after re-dissolving the solid in $CDCl_3$ ($c \approx$ 1 µmol L^{-1}). The spectrum corroborates the formation of the bis(η^2-alkyne)Pt^0 complexes and also reveals a small fraction of free ligands that presumably forms due to the dynamic character of the metal-ligand complexes in dilute solutions.

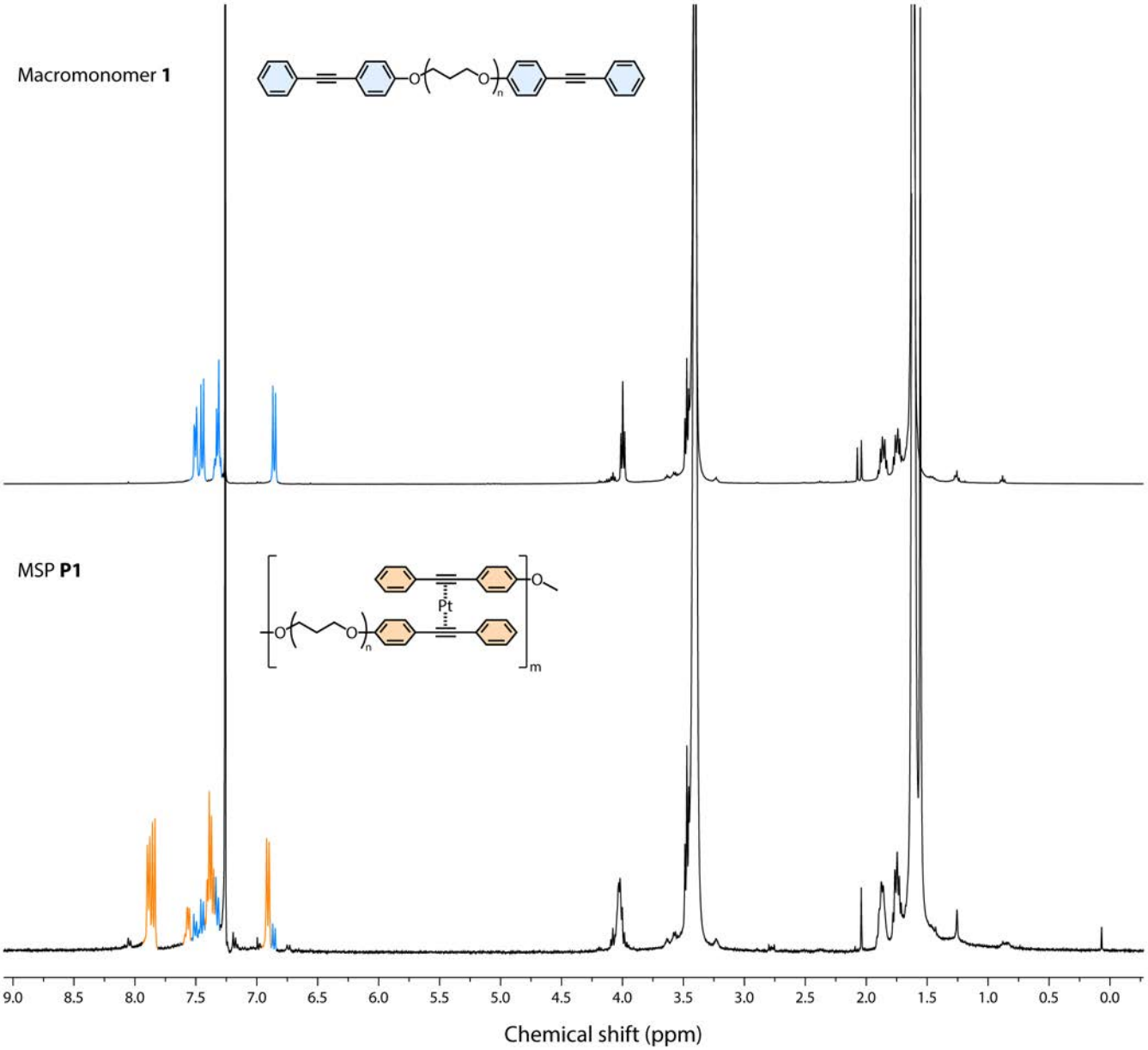

Supplementary Figure S8. Comparison of the ^{1}H-NMR spectra (400 MHz, 297.2 K, $CDCl_3$) of the macromonomer **1** (top) and the corresponding metallosupramolecular polymer **P1** (bottom). The spectrum of **P1** was recorded after re-dissolving a solid sample in $CDCl_3$ ($c \approx 1$ µmol L^{-1}). The characteristic signals of the diphenylacetylene signals of **1** (blue) are shifted in the spectrum of **P1**, corroborating the successful formation of the bis(η^2-alkyne)Pt^0 complexes. The spectrum also reveals a small fraction of free ligands that presumably forms due to the dynamic character of the metal-ligand complexes in dilute solutions.

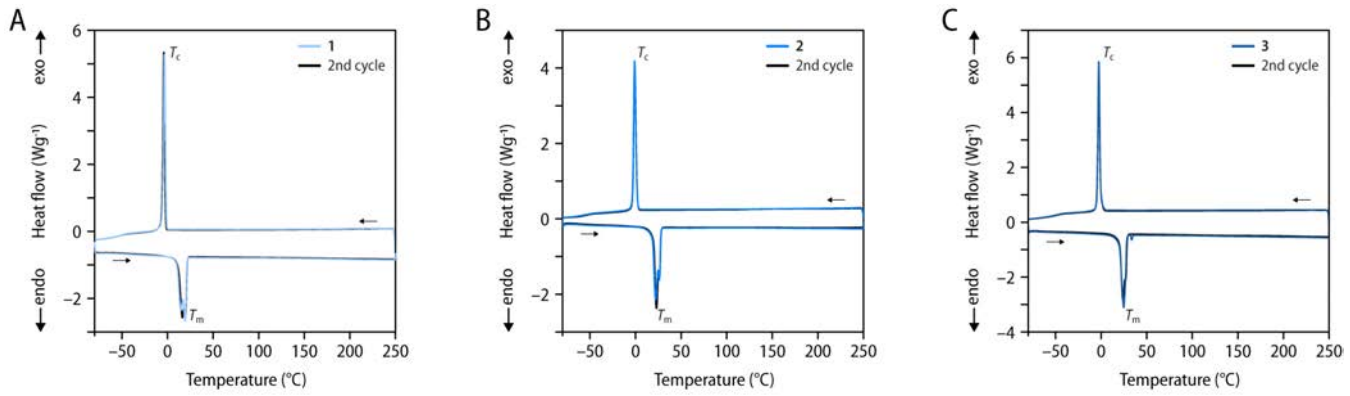

Supplementary Figure S9. Differential scanning calorimetry (DSC) traces of macromonomers (*a*) **1**, (*b*) **2**, and (*c*) **3**. Shown are the first heating and cooling traces (blue) as well as the second heating and cooling traces (black). The first and second DSC heating and cooling traces of **1**–**3** mirror each other and display reversible melting transitions at ca. 19 °C and corresponding crystallization events at ca. −13 °C. The transitions appear to be associated with the crystallization and melting of the poly(tetrahydrofuran) backbone, suggesting the presence of microphase separation between the PTHF and the diphenylacetylene ligands. All DSC experiments were carried out with heating and cooling rates of 10 °C min^{-1}.

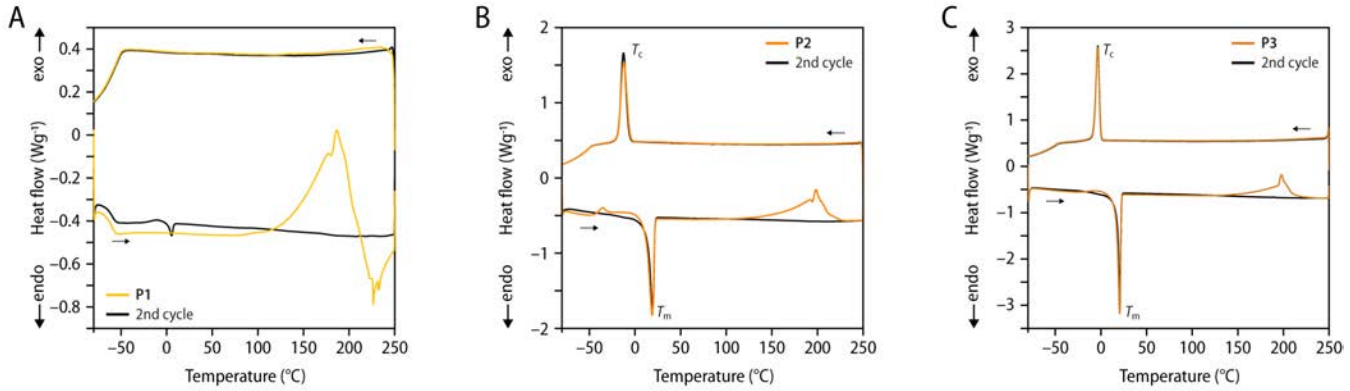

Supplementary Figure S10. Differential scanning calorimetry (DSC) traces of the metallosupramolecular polymers (*a*) **P1**, (*b*) **P2**, and (*c*) **P3**. Shown are first heating and cooling traces (orange) as well as the second heating and cooling traces (black). Samples of **P2** and **P3** display a reversible melting transition at ca. 19 °C, and a corresponding crystallization transition at ca. −13 °C, which can be assigned to the poly(tetrahydrofuran) backbone. A similar weak melting transition is observed in the second heating scan for **P1**. A prominent exothermic transition with an onset at ca. 120 °C and a maximum at >180 °C is observed in the first heating scans of **P1**–**P3**. The exotherm can be assigned to the crosslinking reaction of diphenylacetylene moieties upon dissociation of the Pt-bis(η^2-diphenylacetylene) complexes previously reported for a related metallosupramolecular polymer.[1] All DSC experiments were carried out with heating and cooling rates of 10 °C min^{-1}.

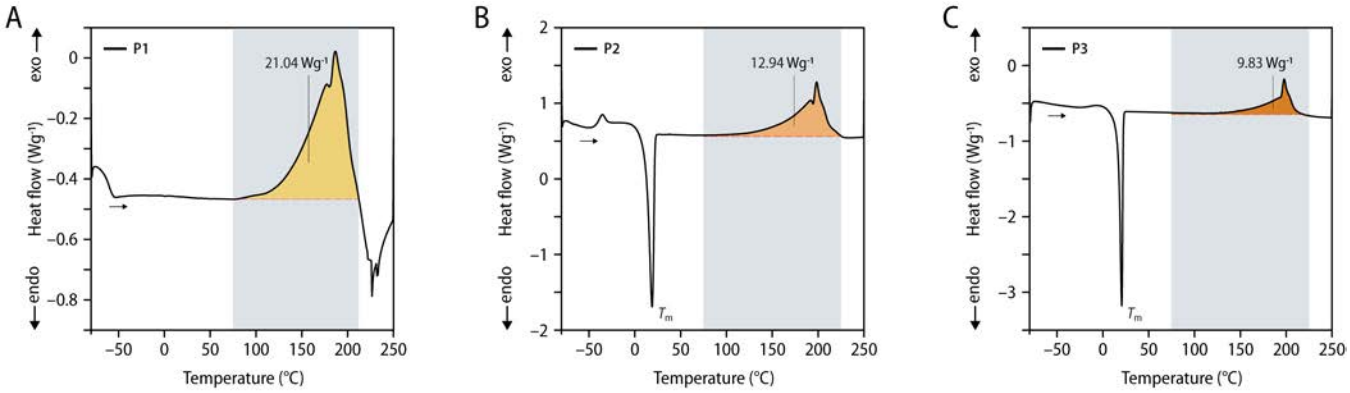

Supplementary Figure S11. Comparison of the first DSC heating traces of the metallosupramolecular polymers (*a*) **P1**, (*b*) **P2**, and (*c*) **P3**. An integration in the temperature interval between 75 and 212 °C was employed to estimate the relative enthalpy of the exothermic processes that occur in this temperature range. The observed reaction enthalpies of (*a*) 21.04, (*b*) 12.9, and (*c*) 9.8 W g^{-1} scale with the weight fraction of the Pt complexes in the MSPs (Table 1).

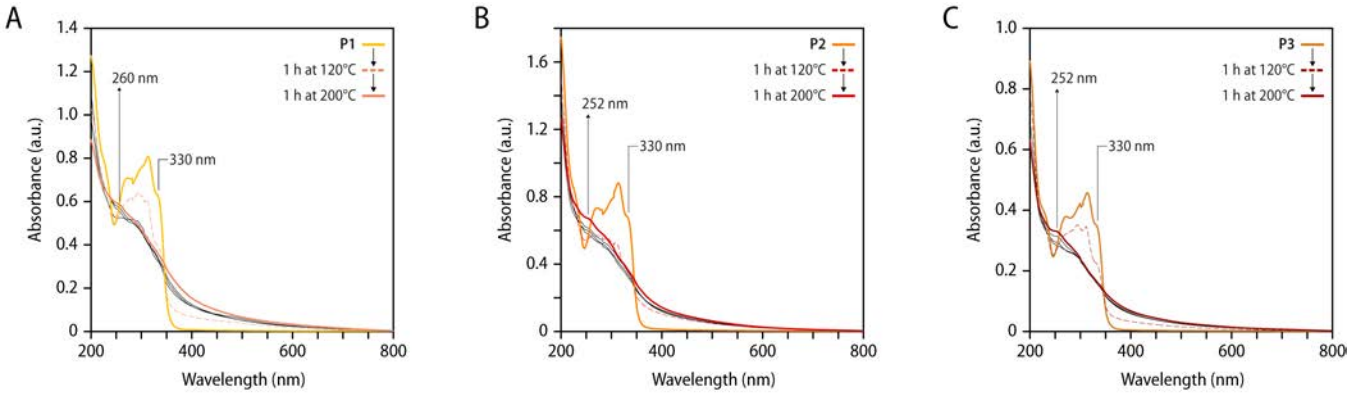

Supplementary Figure S12. UV-vis absorption spectra of thin films of the metallosupramolecular polymers (*a*) **P1**, (*b*) **P2**, and (*c*) **P3**, and spectra recorded after heating in a nitrogen atmosphere to 120 °C for 1 h (violet), to temperatures of 140, 160 and 180 °C (grey), and after annealing at 200 °C for 1 h (black). The films of P1–P3 were prepared by solvent casting $CHCl_3$ solutions (c = 0.02 mol L^{-1}) onto quartz glass substrates. The spectra recorded upon heating of the samples show that the characteristic band of the bis(η^2-alkyne)Pt^0 complexes at 330 nm decreases in intensity while a broad absorption band with a local maximum at ca. 250 nm arises.

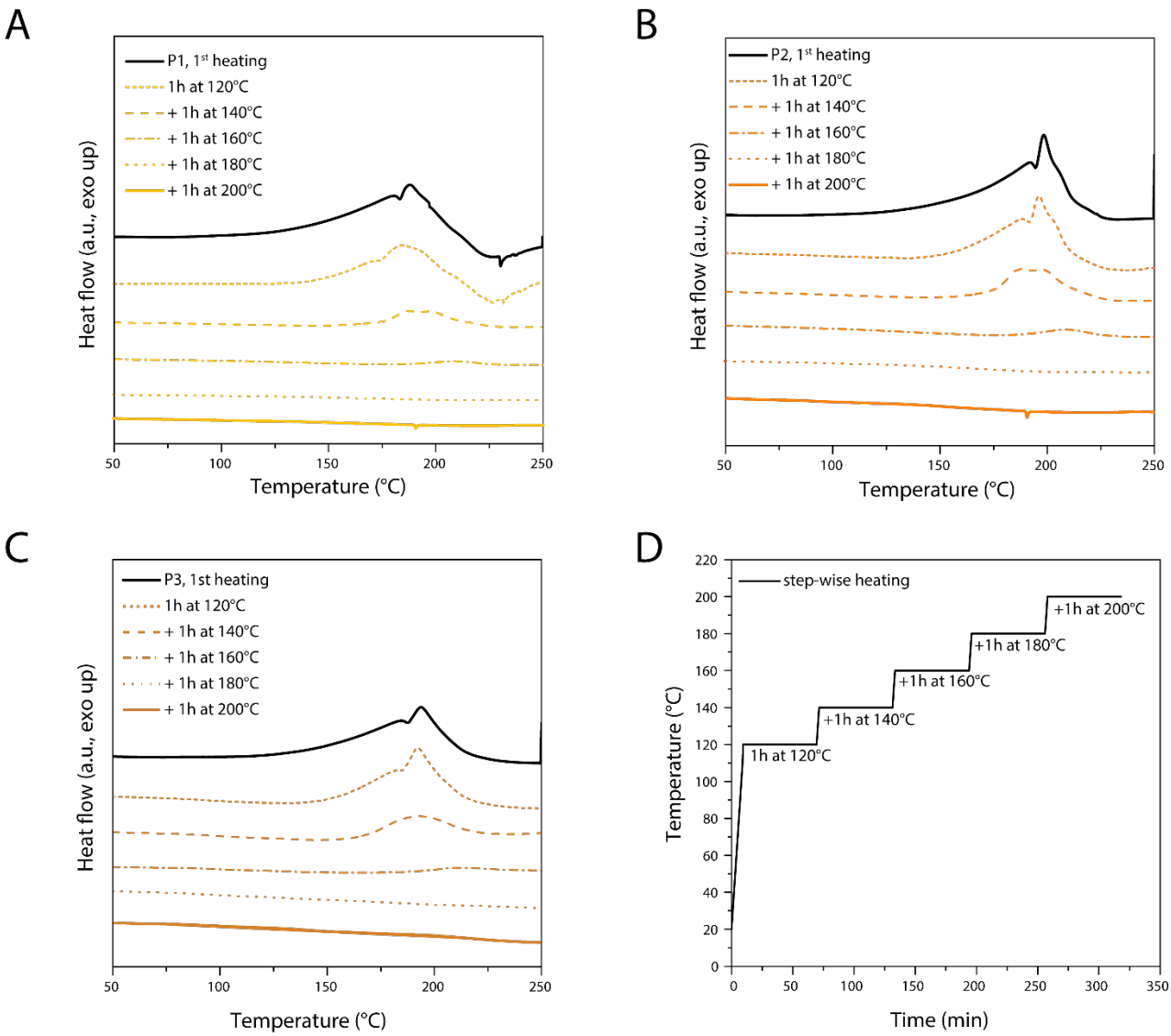

Supplementary Figure S13. Differential scanning calorimetry (DSC) heating traces of solvent-cast samples of the metallosupramolecular polymers (*a*) **P1**, (*b*) **P2**, and (*c*) **P3** recorded after subjecting the samples to different heating protocols. Shown are the first heating trace of a pristine sample (black line) and the heating traces of samples obtained by consecutively heating for 1 h as depicted in (*d*) at temperatures of 120, 140, 160, 180, and 200 °C. The DSC traces show that the exotherm diminished with increased heating to temperatures above 120 °C and is absent after heating samples to temperatures above ca. 160 °C. DSC traces are vertically shifted for clarity.

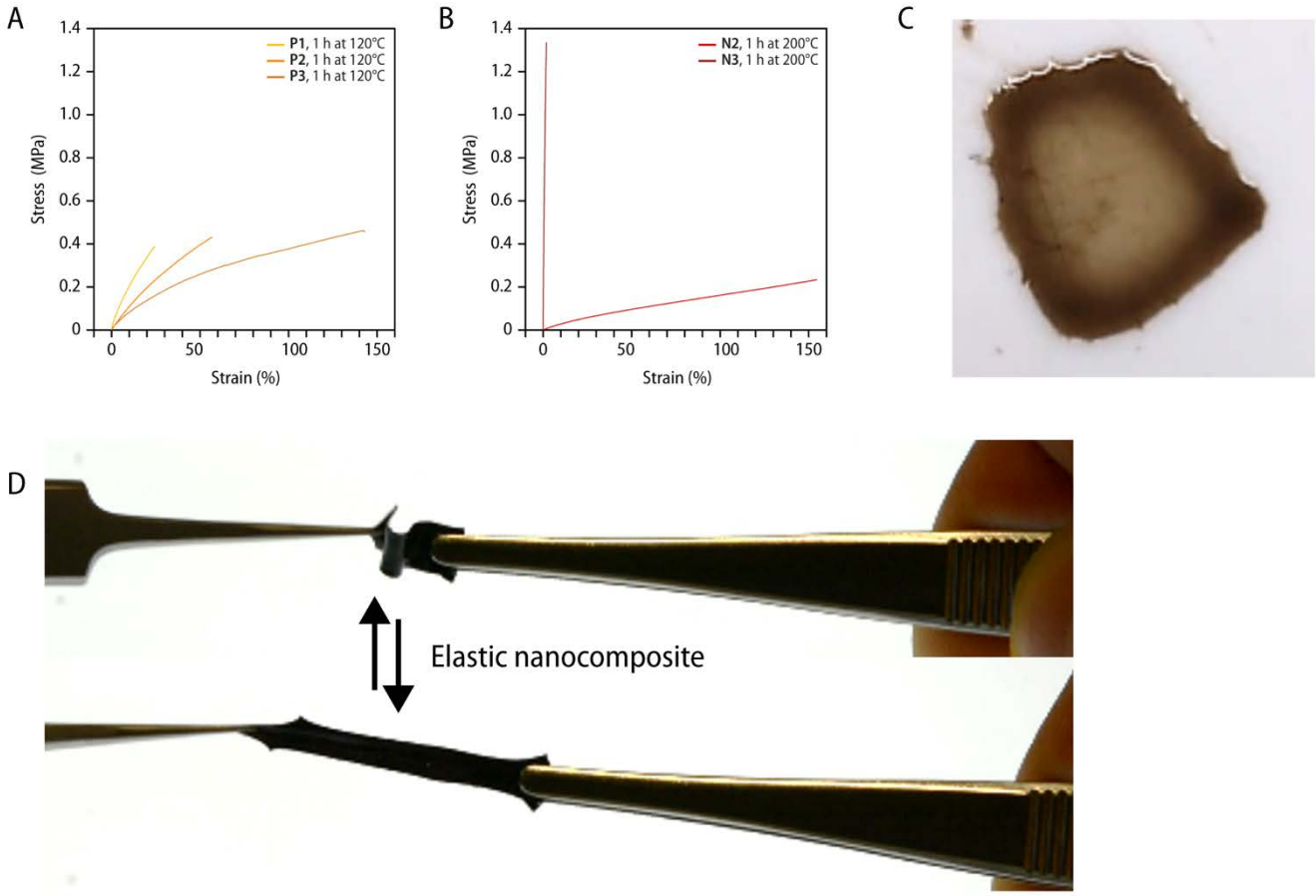

Supplementary Figure S14. (*a*) Comparison of representative stress-strain curves of samples of the nanocomposites **N1**–**N3** that were obtained by heating samples of **P1**–**P3** to a temperature of 120 °C for 1 h in an inert atmosphere. (b) Comparison of representative stress-strain curves of samples of the nanocomposites **N2**–**N3** that were obtained by heating samples of **P2**–**P3** to a temperature of 200 °C for 1 h in an inert atmosphere. Samples of **P1** that were heated to a temperature of 200 °C for 1 h underwent brittle failure prior to testing. All uniaxial tensile tests were carried out with dog-bone shaped samples with approximate dimensions of 15 × 3 × 0.2 cm (length × width × thickness) that were cut from films of the nanocomposites and a strain rate of strain rate of 5 % min^{-1}. (*c*) Photograph of a drop-cast sample of **P3** prior to heating. (*d*) Photographs showing the elastic nanocomposite **N3** obtained after compression molding films of **P3** at a temperature of 120 °C for 1 h.

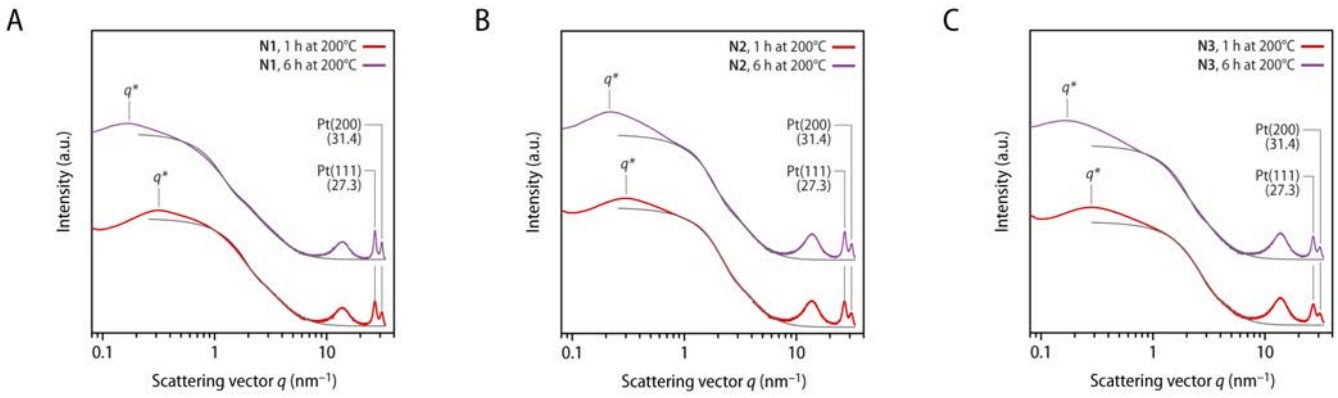

Supplementary Figure S15. Characterization of samples of the nanocomposites **N1**–**N3** by small- and wide-angle X-ray scattering. *a*–*c*) Scattering profiles recorded for samples of **N1**–**N3** after heating to a temperature of 200°C for 1 h and 6 h. The grey lines are the form factors of polydisperse spheres[1] with radii (R_P) of (*a*) 1.5 ± 0.4 nm (1 h) and 2.4 ± 0.6 nm (6 h), (*b*) 1.3 ± 0.4 nm (1 h) and 1.5 ± 0.4 nm (6 h), as well as (*c*) 1.1 ± 0.4 nm and 1.4 ± 0.4 nm (6 h). The indicated q^* values were used to calculate the nearest neighbor distances $\boldsymbol{d}_{\mathbf{nn}}^{\mathbf{exp}}$ reported in Table 2. Scattering curves are vertically shifted for clarity. The broad maximum observed in the scattering profiles at ca. 12–16 nm^{-1} corresponds to the amorphous halo and the background of the polyimide (Kapton) substrate.

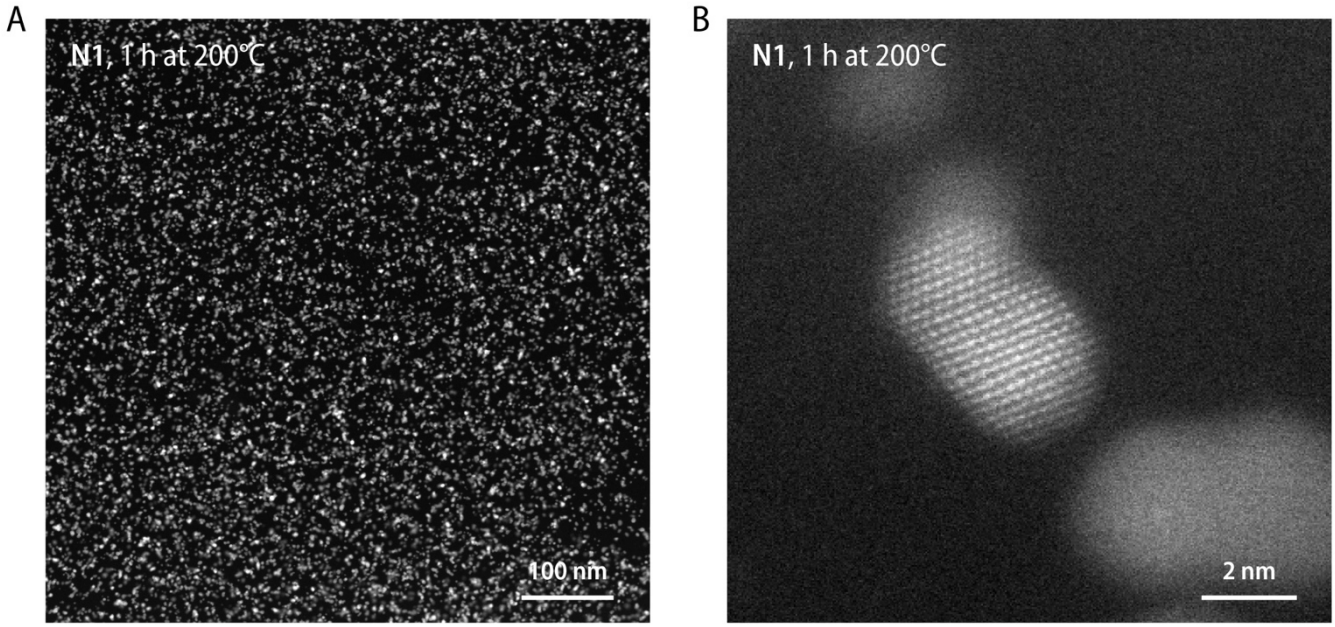

Supplementary Figure S16. *a,b)* High-angle annular dark-field (HAADF) scanning transmission electron microscopy (STEM) images of a sample of **N1** recorded after heating at 200 °C for 1 h. The micrographs show Pt-NPs distributed in the nanocomposite and the micrograph in (*b*) shows the lattice fringes of an individual crystalline particle.

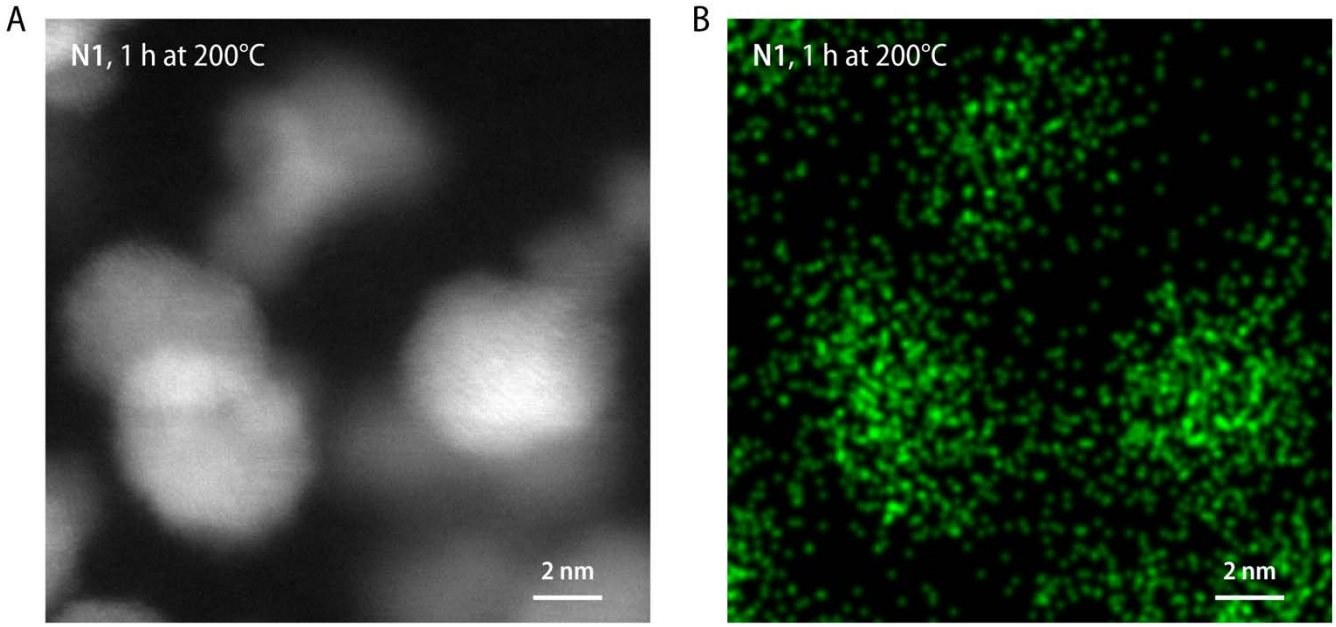

Supplementary Figure S17. *a)* High-angle annular dark-field (HAADF) scanning transmission electron microscopy (STEM) images of a sample of **N1** recorded after heating at 200 °C for 1 h. *b*) Energy-dispersive X-ray spectroscopy elemental map for platinum (green) for the STEM micrograph shown in (*a*).

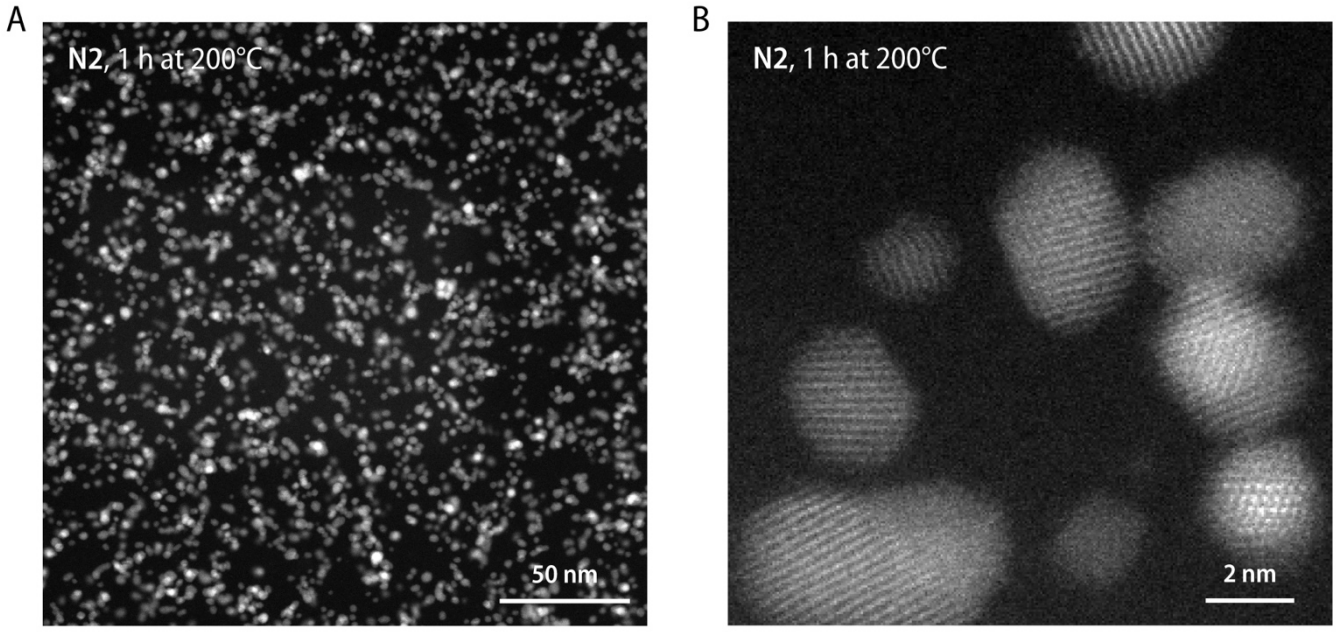

Supplementary Figure S18. *a,b)* High-angle annular dark-field (HAADF) scanning transmission electron microscopy (STEM) images of a sample of **N2** recorded after heating at 200 °C for 1 h. The micrographs show Pt-NPs distributed in the nanocomposite and the micrograph in (*b*) shows the lattice fringes of individual crystalline particles.

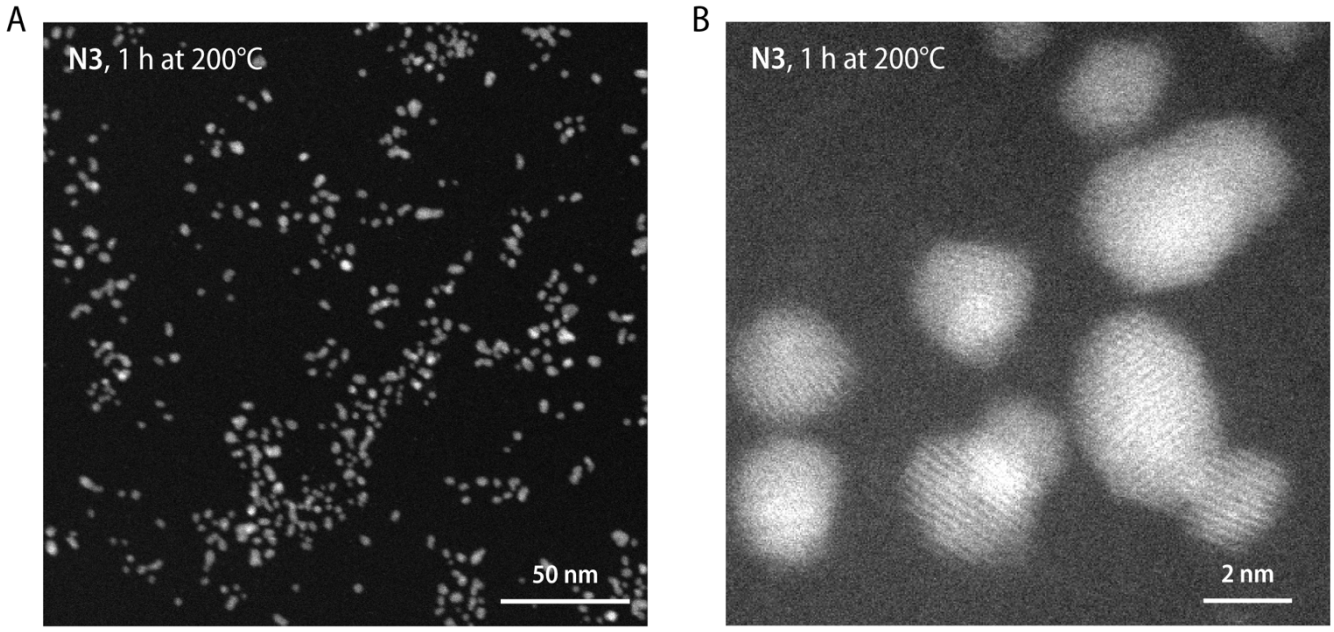

Supplementary Figure S19. *a,b)* High-angle annular dark-field (HAADF) scanning transmission electron microscopy (STEM) images of a sample of **N3** recorded after heating at 200 °C for 1 h. The micrographs show Pt-NPs distributed in the nanocomposite and the micrograph in (*b*) shows the lattice fringes of individual crystalline particles.

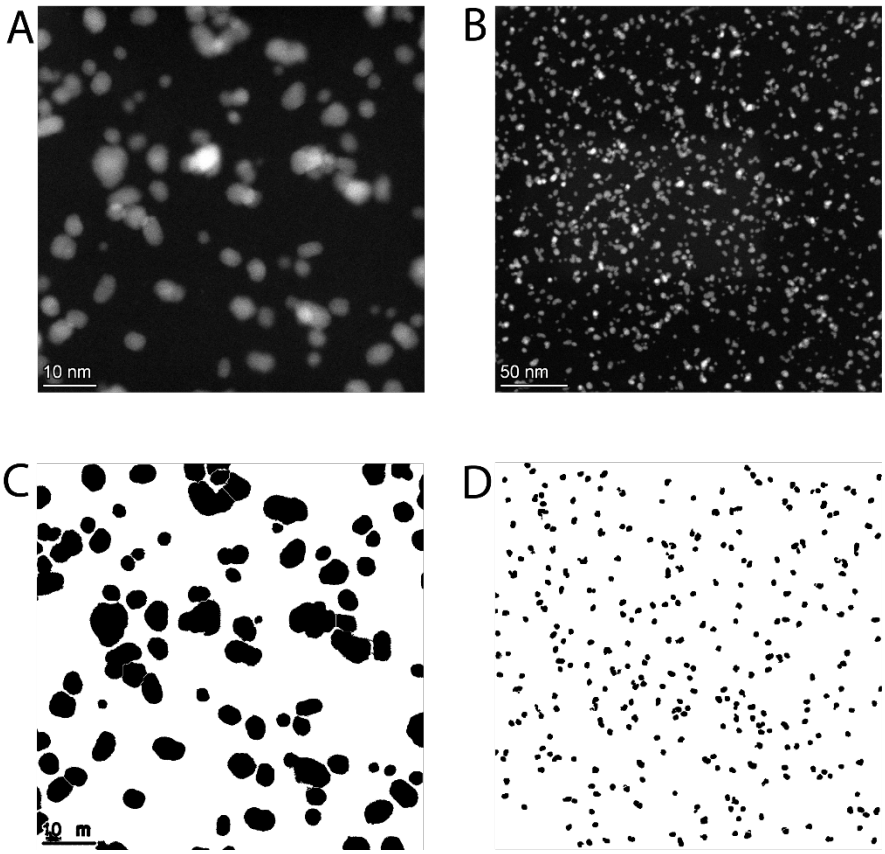

Supplementary Figure S20. (*a, b*) STEM images recorded after heating samples of **P1** at a temperature of 200 °C for 1 h and (*c, d*) results of the segmentation algorithm that was performed with these STEM images of **N1**. The segmentation algorithm was performed to carry out a dimensional analysis of the average radii of the Pt nanoparticles obtained in the different samples.

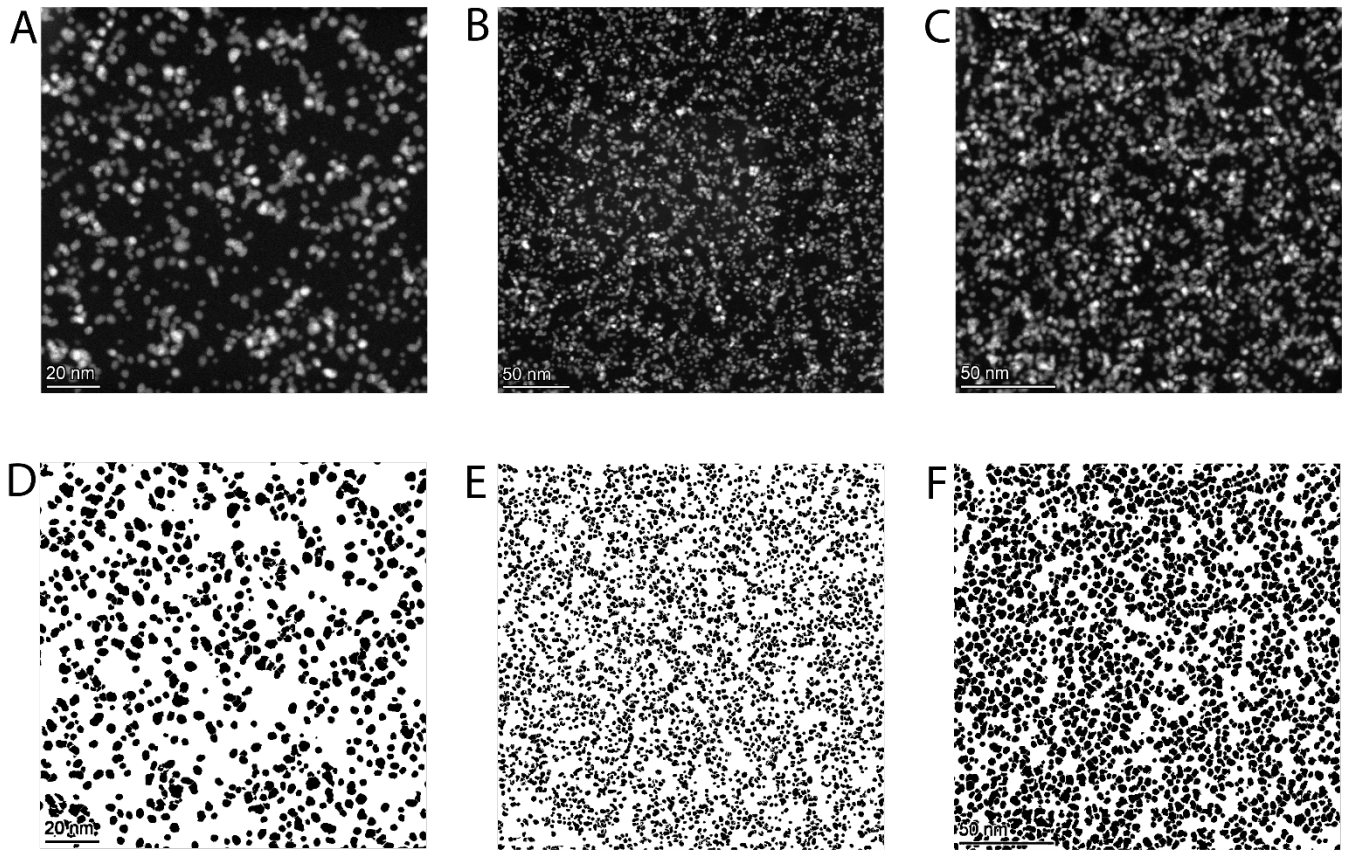

Supplementary Figure S21. (*a*–*c*) STEM images recorded after heating samples of **P2** at a temperature of 200 °C for 1 h and (*d*–*f*) results of the segmentation algorithm that was performed with these STEM images of **N2**. The segmentation algorithm was performed to carry out a dimensional analysis of the average radii of the Pt nanoparticles obtained in the different samples.

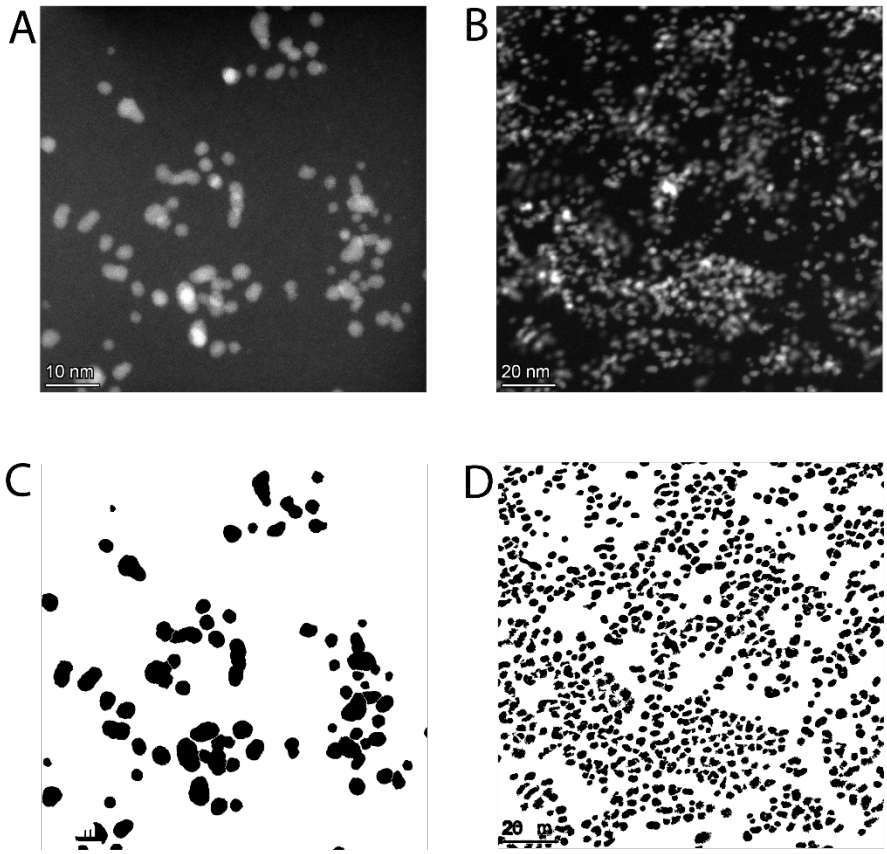

Supplementary Figure S22. (*a, b*) STEM images recorded after heating samples of **P3** at a temperature of 200 °C for 1 h and (*c, d*) results of the segmentation algorithm that was performed with these STEM images of **N3**. The segmentation algorithm was performed to carry out a dimensional analysis of the average radii of the Pt nanoparticles obtained in the different samples.

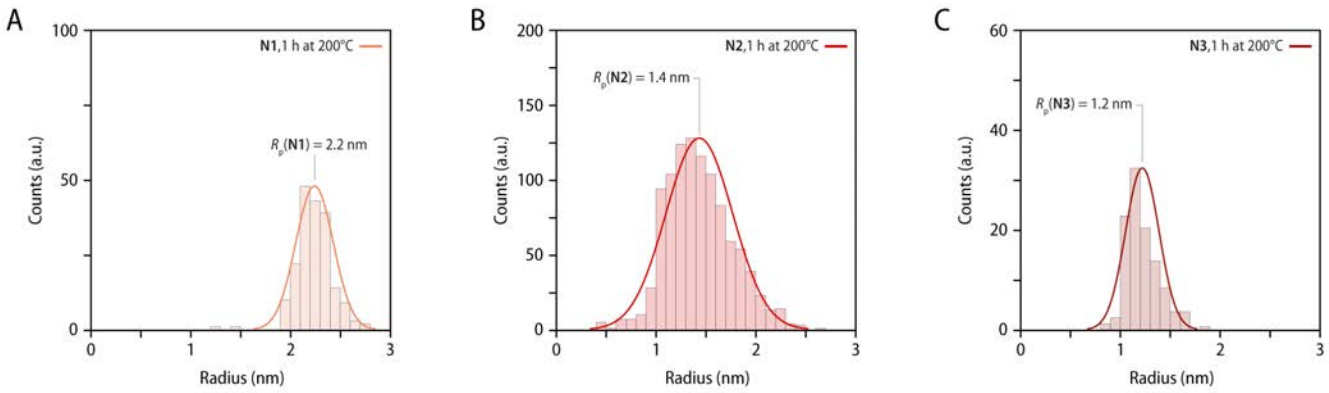

Supplementary Figure S23. Size distribution of Pt-NPs in **N1**–**N3** as determined by analysis of the STEM images with a segmentation algorithm (see Figures S15). The particle radii were determined by means of the area density and the roundness, which were calculated by image analysis of over 100 particles. Average radii of the Pt-NPs were determined as (*a*) 2.2 ± 0.2 nm for **N1**, (*b*) 1.4 ± 0.3 nm for **N2**, and (*c*) 1.2 ± 0.2 nm for **N3**.

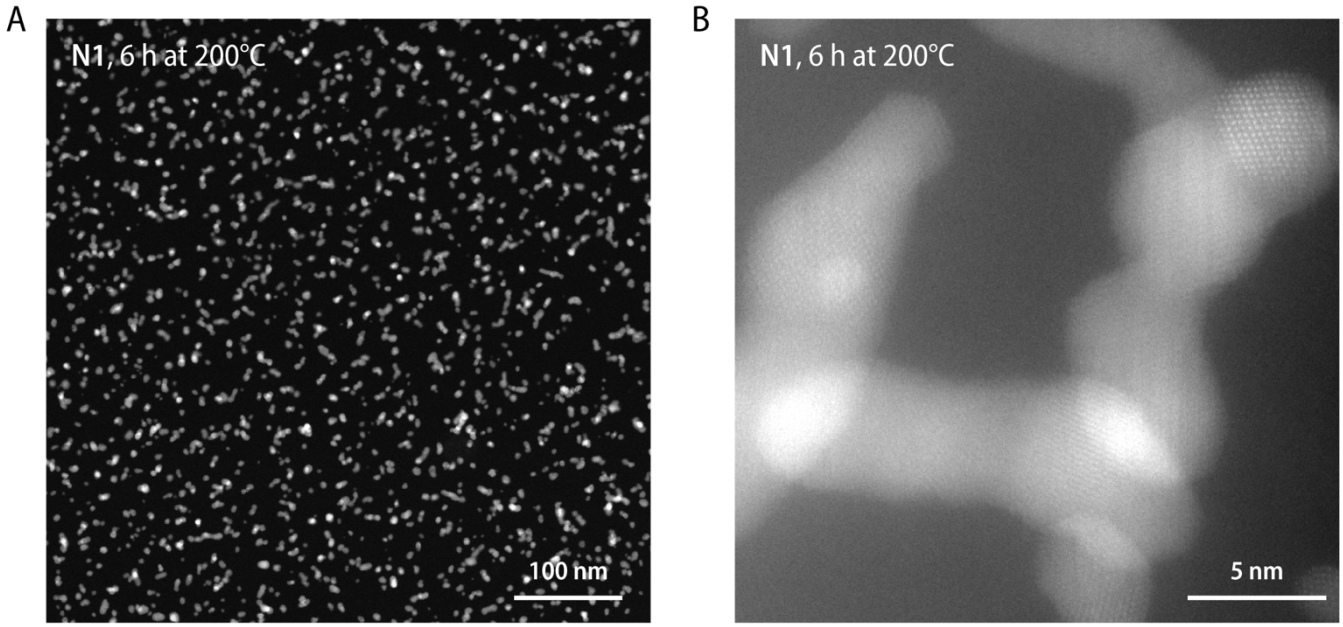

Supplementary Figure S24. *a,b*) High-angle annular dark-field (HAADF) scanning transmission electron microscopy (STEM) images of a sample of **N1** recorded after heating at 200 °C for 6 h. The micrographs show Pt-NPs distributed in the nanocomposite and the micrograph in (*b*) shows the lattice fringes of individual crystalline particles.

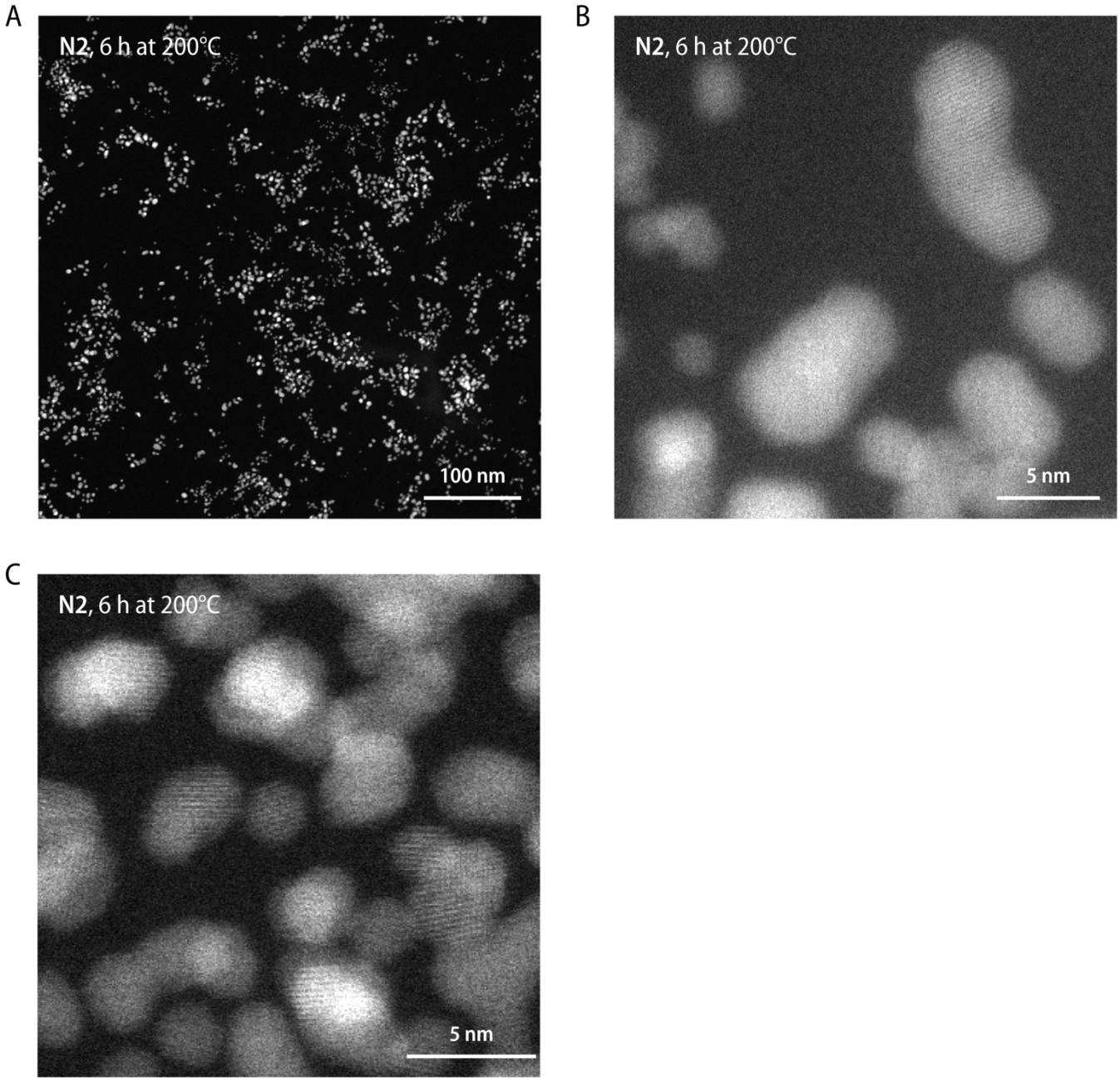

Supplementary Figure S25. *a–c*) High-angle annular dark-field (HAADF) scanning transmission electron microscopy (STEM) images of a sample of **N2** recorded after heating at 200 °C for 6 h. The micrographs show Pt-NPs distributed in the nanocomposite and the micrographs in (*b,c*) shows the lattice fringes of an individual crystalline particles.

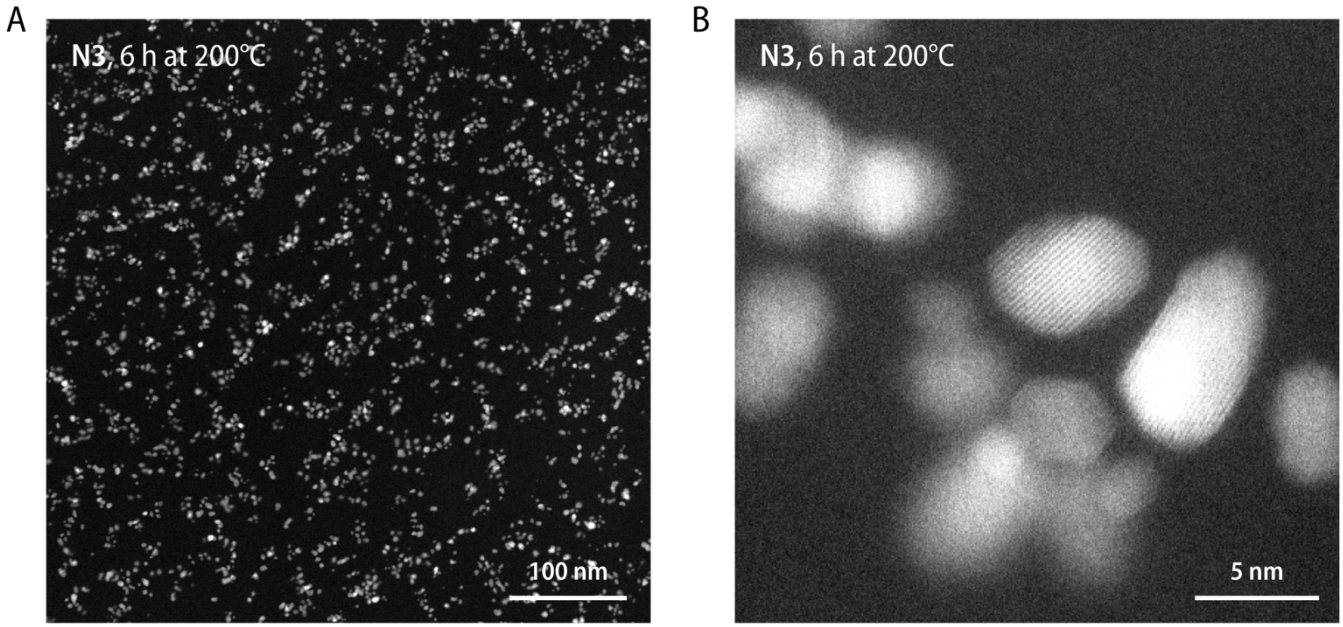

Supplementary Figure S26. *a,b*) High-angle annular dark-field (HAADF) scanning transmission electron microscopy (STEM) images of a sample of **N3** recorded after heating at 200 °C for 6 h. The micrographs show Pt-NPs distributed in the nanocomposite and the micrograph in (*b*) shows the lattice fringes of individual crystalline particles.

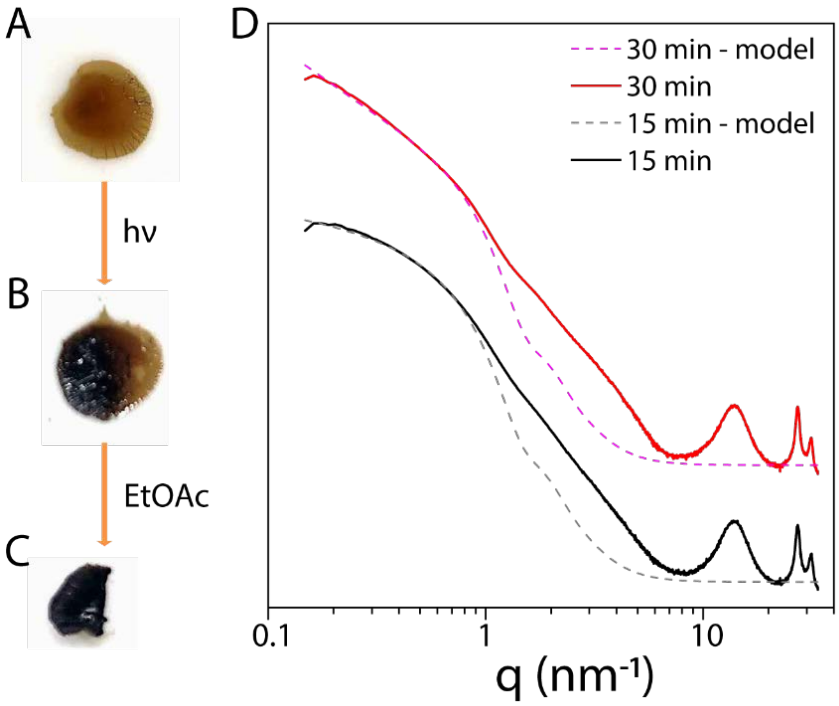

Supplementary Figure S27. (*a*–*c*) Photographs showing the photolithographic processing of the metallosupramolecular polymer. Photographs of (*a*) a sample of **P2** that was solvent-cast on a polytetrafluoroethylene substrate (thickness ca. 100 μm) and (*b*) the same sample after partial irradiation with UV light (15 min, 320–390 nm, 900 mW cm^{-2}). A part of the sample was covered with aluminum foil to shield it from the UV irradiation. (*c*) Photograph of the sample after selective removal of the unexposed sample regions by rinsing with ethyl acetate (ca. 10 mL). (*d*) Small- and wide-angle X-ray (SAXS/WAXS) scattering profiles of samples of **N2** after exposure to UV light irradiation (320–390 nm, 900 mW cm^{-2}) for 15 and 30 min and comparison with computed profiles of fractal aggregates with the indicated fractal dimensions (d_f) and particles radii (R_p). The scattering data also show scattering peaks at 27.3 and 31.4 nm^{-1} that correspond to 2θ values of 39.09 and 45.44°, in excellent agreement with the expected positions for the reflections of the (111) and (200) plane of Pt-NPs with a face-centered cubic crystal structure. Scattering curves are vertically shifted for clarity. The broad maximum observed in the scattering profiles at ca. 12–16 nm^{-1} corresponds to the amorphous halo and the background of the polyimide (Kapton) substrate.

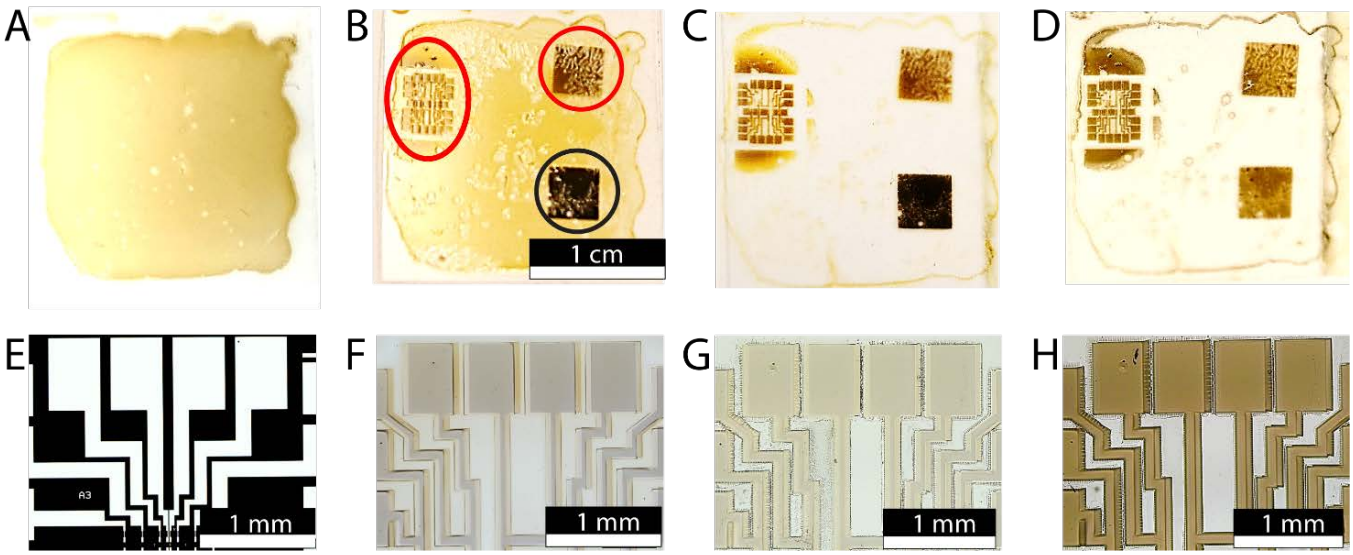

Supplementary Figure S28. (*a*) Photograph of a thin film of **P2** (ca. 30 µm) that was spin-coated on a quartz glass substrate. (*b*) Photograph of the film of **P2** after exposure to UV irradiation (320–390 nm; 900 mW cm^{-2}) through a photomask for 15 min (red circles) or 30 min (black circle). (*c*) Photograph of the sample after selective removal of non-exposed sample regions by rinsing with ethyl acetate and (*d*) after heating the rinsed and dried sample to a temperature of 200 °C for 1 hour in inert nitrogen atmosphere. (*e*) Optical microcopy image of a feature of the chrome photomask that was used to selectively irradiate samples of the metallosupramolecular polymer (**P1**–**P3**). (*f*–*h*) Micrographs of the section of the film of P2 that was exposed to UV light irradiation through the part of the photomask shown in (e). The micrographs show (*f*) the film of **P2** after exposure to UV light (15 min, 320–390 nm; 900mW cm^{-2}), (*g*) after subsequent rinsing with ethyl acetate, and (*h*) after finally heating the sample in an inert nitrogen atmosphere to 200 °C for 1 hour. The micrographs corroborate a successful replication of the features of the photomask in a nanocomposite through the photolithographic processing of a sample of the metallosupramolecular polymer.

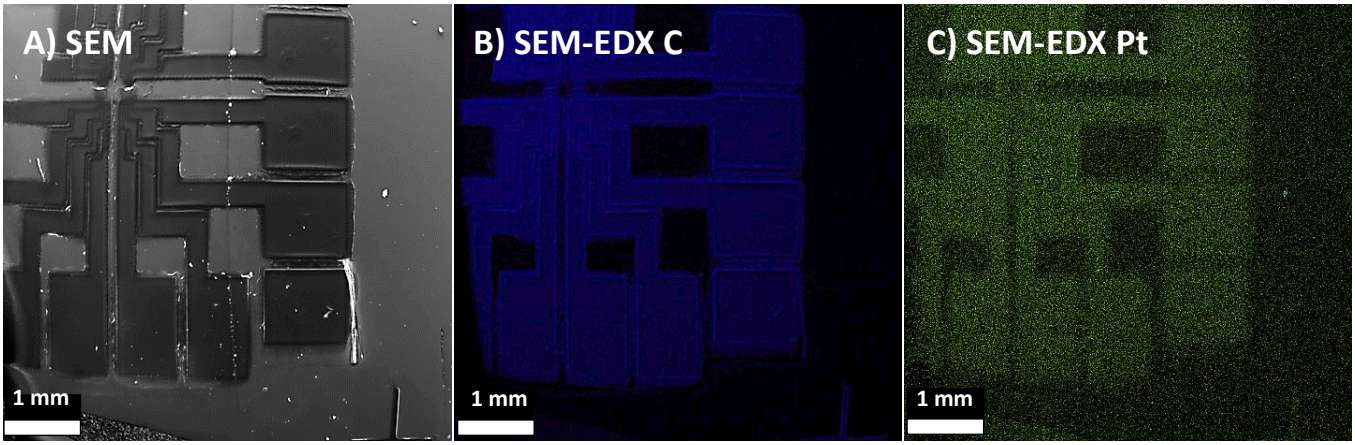

Supplementary Figure S29. (*a*) Scanning electron microscopy (SEM) image of a sample of **N1** obtained by UV irradiation through a photomask and subsequent removal of the non-irradiated sample region by rinsing with ethyl acetate. (*b*–*c*) Energy dispersive X-ray (EDX) imaging of the sample region shown in (*a*) with the signal for (*b*) carbon and (*c*) platinum. The imaging by SEM-EDX corroborates that irradiation and washing allows to photolithographically prepared the Pt-nanocomposite with a controlled structure.

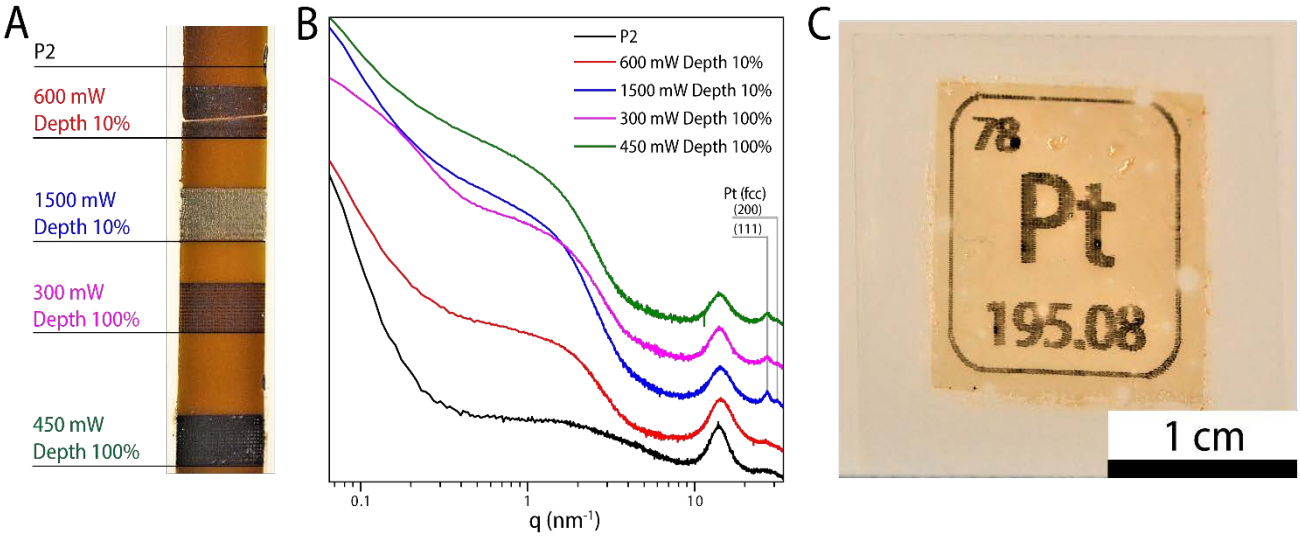

Supplementary Figure S30. (*a*) Photograph (top-view) of a solvent-cast film of **P2** (thickness ca. 100 µm) with sample regions that were exposed to laser irradiation by a laser engraving machine (400–460 nm) with the indicated intensity to induce the nanocomposite formation. (*b*) SAXS-WAXS scattering profiles recorded in the different irradiated areas. The scattering profiles indicate that laser irradiation at the absorption edge of the metallosupramolecular polymer is sufficient to induce the nanocomposite formation, as corroborated by the observed scattering peaks at ca. 27.3 and 31.4 nm^{-1}, in excellent agreement with the expected positions for the reflections of the (111) and (200) plane of Pt-NPs with a face-centered cubic crystal structure. (*c*) Photograph of a solvent-cast film of **P2** that was exposed to laser irradiation (laser power 450 mW (15%), depth 100%) to create a defined pattern.

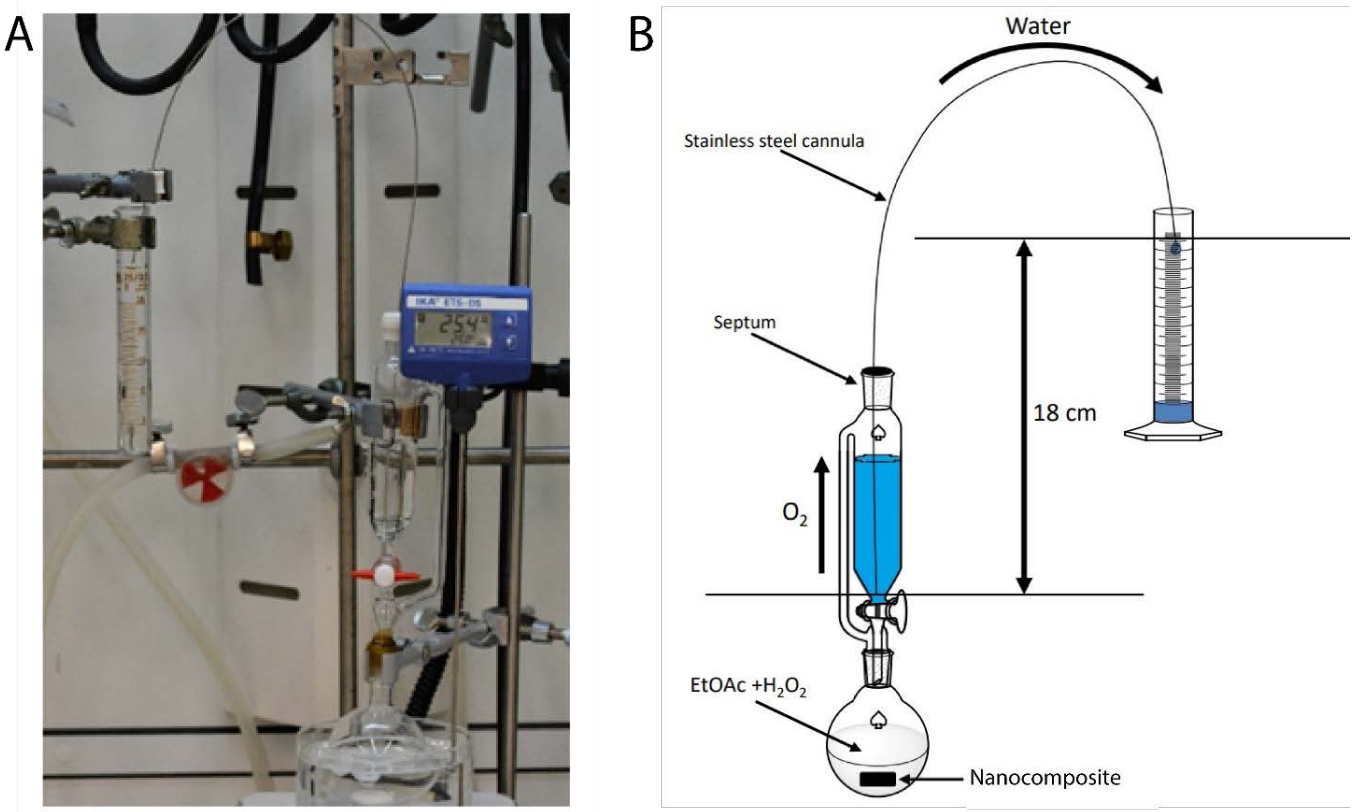

Supplementary Figure S31. (*a*) Photograph and (*b*) schematic depiction of the setup employed to volumetrically determine the gas evolution from the Pt-NP catalyzed decomposition reaction of hydrogen peroxide and ammonium borate. The nanocomposite material was immersed in a flask containing either aqueous or ethyl acetate solutions containing hydrogen peroxide or ammonium borate. The evolving oxygen or hydrogen gas upon decomposition of H_2O_2 or NH_3BH_3 results in an overpressure that displaces water from the dropping funnel into a volumetric flask. The amount of displaced water was measured to determine the rate of gas evolution.

2. Supplementary Tables S1–S5

Supplementary Table S1. Comparison of the residual masses at a temperature of 600 °C as observed by thermogravimetric analysis measurements with samples of macromonomers **1**–**3** and samples of the metallosupramolecular polymers **P1**–**P3**. Also given are the calculated weight fractions of platinum in the samples of the MSPs.

Sample	**Residue at 600 °C** (wt%)[a]	**Calculated Pt in samples** (wt%)[b]
1	2.2 ± 0.4	–
2	1.7 ± 1.1	–
3	1.1 ± 1.0	–
P1	15.8 ± 1.7	13.6 ± 1.8
P2	12.8 ± 2.4	11.1 ± 2.6
P3	9.3 ± 2.1	8.2 ± 2.4

[a] Data represent the averages of 3 measurements and given is the residual sample mass after heating samples at 10 °C min^{-1} up to a temperature of 600 °C. The values are given ± standard deviation (std). [b] Data represent the weight fraction of platinum in the MSPs as determined by subtraction of the residual mass of **1**–**3** from the residual mass of MSPs **P1**–**P3** with standard deviations (std) given as $\pm \sqrt{(std\ \text{macromonomer})^2 + (std\ \text{MSP})^2}$.

Supplementary Table S2. Overview of characteristics of the Pt nanoparticles as determined experimentally by small- and wide-angle X-ray scattering (SAXS/WAXS) and scanning transmission electron microscopy (STEM).

Sample	Prep. protocol	Volume fraction Pt	Particle radius		Particle spacing			STEM image analysis	
			SAXS	STEM	Theory	SAXS	STEM	Area density	Roundness
		φ_P[a]	R_P (nm)[b]	R_P (nm)[c]	d_{nn}^{pred} (nm)	d_{nn}^{exp} (nm)[d]	(nm)[e]	(%)[f]	(%)[f]
N1	200 °C / 1 h	0.0078	2.6 ± 0.8	2.2 ± 0.2	15.1	20	6.2 ± 2.0	26.8	80.4
	200 °C / 6 h		3.7 ± 1.1	–	24.2	36	12.7 ± 4.9	21.2	66.5
N2	200 °C / 1 h	0.0041	1.8 ± 0.5	1.4 ± 0.3	16.1	21	8.0 ± 3.0	19.4	83.9
	200 °C / 6 h		2.1 ± 0.6	–	20.2	29	15.1 ± 6.0	11.6	71.8
N3	200 °C / 1 h	0.0025	1.7 ± 0.5	1.2 ± 0.2	16.2	22	12.0 ± 6.5	9.0	82.7
	200 °C / 6 h		1.9 ± 0.6	–	20.6	33	18.0 ± 8.0	8.9	72.1

[a] The theoretical particle volume fraction (φ_P) was calculated assuming that the particles are non-disperse and using the density values ρ_{Pt} = 21.45 g cm^{-3} and ρ_{PTHF} = 1.00 g cm^{-3}. of 2.6 ± 0.8, 1.8 ± 0.5, and 1.7 ± 0.5 nm. [b] Data represent the particle radii as determined by fitting the scattering profiles with theoretical models for the scattering of fractal aggregates. [c] The mean particle radius was calculated from the STEM images by image analysis of over 100 particles and the values are given ± standard deviation. [d] The particle spacing was determined from the maximum of the main scattering peak q^* in the SAXS region and calculated as $d = 2\pi/q$. [e] The mean particle distance was calculated from the STEM images by image analysis of over 100 particles and the values are given ± standard deviation. [f] The area density and the roundness were calculated from the STEM images by image analysis of over 100 particles.

Supplementary Table S3. Mechanical properties of samples of **N1**–**N3** with a varying processing history, i.e., films that were compression molded at 120 °C (3 tons, 1 h) and samples that were subsequently heated at 200 °C for 1 h in an inert nitrogen atmosphere.

Sample	Treatment	Young's modulus (kPa) [a]	Tensile strength (kPa) [a]	Strain at break (%) [a]	Toughness (kJ m^{-3}) [a]
N1	120 °C / 1 h	20.0 ± 7.7	389.5 ± 62.4	35 ± 13	7.9 ± 4.1
	200 °C / 1 h	n.d.	n.d.	n.d.	n.d.
N2	120 °C / 1 h	10.4 ± 0.9	298.7 ± 117.8	42 ± 14	7.9 ± 5.4
	200 °C / 1 h	2.7 ± 0.1	188.2 ± 42.8	119 ± 34	13.1 ± 6.3
N3	120 °C / 1 h	8.6 ± 1.3	485.3 ± 91.7	125 ± 17	35.9 ± 9.3
	200 °C / 1 h	1375.7 ± 1213.5	951.0 ± 386.2	1.0 ± 0.8	0.7 ± 0.7

[a] Stress-strain experiments were carried out at 25 °C with a strain rate of 5 % min^{-1}. Data represent averages of n = 3 individual measurements ± standard deviation.

Supplementary Table S4. Overview of the rates of gas evolution from the nanocomposite-catalyzed decomposition reactions of hydrogen peroxide and ammonia borane. **N1**–**N3** (200 °C, 1 h) were used as dip catalysts in solution of H_2O_2 in ethyl acetate ($c(H_2O_2)$ = 7.3 mol L^{-1}) or water ($c(H_2O_2)$ = 7.3 mol L^{-1}), as well as in solutions of NH_3BH_3 in water ($c(H_2O_2)$ = 7.3 mol L^{-1}).

Sample	**H_2O_2 in ethyl acetate** (μmol min^{-1} mg^{-1})	**H_2O_2 in water** (μmol min^{-1} mg^{-1})	**NH_3BH_3 in water** (μmol min^{-1} mg^{-1})
N1 – 1h / 200 °C	517	1.6	4.2
N2 – 1h / 200 °C	405	1.5	1.5
N3 – 1h / 200 °C	398	1.4	0.8

[a] The rate of gas evolution was determined by volumetric measurements with the setup depicted in Supplementary Figure S29.

Supplementary Table S5. Comparison of the number-average molecular weights (M_n) determined by ^{1}H-NMR spectroscopy. To determine the M_n ,the integration of the doublet signal associated with the protons of the phenyl ring at 6.95 ppm was used for **1–3**, and the triplet associated with the protons of the terminal –CH_2–O– at 3.64 ppm was used for the analysis of the poly(tetrahydrofuran) (PTHF) samples, in each case against the multiplet of the polymer backbone centered at ca. 3.53 ppm.

Sample	M_n **by NMR** (g mol^{-1})
PTHF 1000 g mol^{-1}	858
1	1896
PTHF 2000 g mol^{-1}	2192
2	3425
PTHF 2000 g mol^{-1}	3289
3	4604

3. Materials and Methods

Chemical Analytics. NMR spectroscopy was carried out at 297.2 K on Bruker Avance III 400 or 300 spectrometers at frequencies of 400 or 300 MHz, respectively, for ^{1}H nuclei in $CDCl_3$. Spectra were calibrated to the residual solvent peak of $CDCl_3$ (7.26 ppm ^{1}H NMR), chemical shifts (δ) are expressed in parts per million (ppm) relative to tetramethylsilane, and coupling constant are given in Hz (multiplicity: *s* = singlet, *d* = doublet, *dd* = double doublet, *t* = triplet, *m* = multiplet). Matrix assisted laser desorption/ionization (MALDI) time-of-flight (TOF) mass spectrometry was performed as service measurements by the Analytical Services of the Chemistry Department of the University of Fribourg on a Bruker UltrafleXtreme MALDI-TOF with *trans*-2-[3-(4-*tert*-butylphenyl)-2-methyl-2-propenylidene]malononitrile (DCTB) as matrix. Size exclusion chromatography (SEC) was performed on an Agilent 1200 series HPLC system equipped with an Agilent PLgel mixed guard column (particle size = 5 µm) and two Agilent PLgel mixed-D columns (*ID* = 7.5 mm, *L* = 300 mm, particle size = 5 µm). Signals were recorded by a UV detector (Agilent 1200 series), an Optilab REX interferometric refractometer, and a miniDawn TREOS light scattering detector (Wyatt Technology Corp.). THF was used as the eluent at a flow rate of 1 mL min^{-1}. Data analyses were carried out with the Astra software suite (Wyatt Technology Corp.) and molecular weights were determined based on narrow molecular weight poly(methyl methacrylate) standards.

UV-vis Spectroscopy and Spectrophotometric Titrations. UV-vis absorption spectroscopy was performed on a Shimadzu UV-2401 PC spectrophotometer with quartz glass cuvettes from Hellma with a path length of 1 cm. Spectrophotometric titrations were carried out with solutions of the macromonomers **1**–**3** ($c(CHCl_3)$ = 12.6, 10.9 and 16.3 mmol L^{-1}, respectively). To the solution of the respective macromonomer (1.8 mL), aliquots (each aliquot: 4 µL, total volume added: 64, 80, and 72 µL, respectively) of a $Pt^0(styrene)_3$ solution ($c(CHCl_3)$ = 0.7, 0.8 and 1.1 mmol L^{-1}, for titrations with **1**–**3**, respectively) were added. After each addition of an aliquot of the $Pt^0(styrene)_3$ solution the mixture was stirred for 30 s for equilibration prior to recording an absorption spectrum. The formation of the complexes was followed by addition of each aliquot of the $Pt^0(styrene)_3$ solution and the absorption intensity at the characteristic wavelength associated with the metal-ligand charge transfer band at 330 nm was monitored. To determine the concentrations of $Pt^0(styrene)_3$ solutions, a similar procedure was performed with the ligand 1-hexyloxy-4-phenylethynyl benzene ($c(CHCl_3)$ = 30 µmol L^{-1}) and $Pt^0(styrene)_3$, as previously reported.[2]

Thermal Characterization. Differential scanning calorimetry (DSC) measurements were carried out on a Mettler Toledo DSC1 Star system operating under a nitrogen atmosphere with 40 µL alumina pans and heating and cooling rates of 10 °C min^{-1} in the temperature range between –80 °C and 250 °C. Unless otherwise indicated, a sample mass of ca. 5 mg was employed. The midpoint of the step change in the heat capacity is reported as the glass transition temperature (T_g) and the melting temperature (T_m) is reported based on the minimum of the major endothermic melting peak. Thermogravimetric analysis (TGA) was performed in a PerkinElmer TGA 4000 in air with 40 µL alumina pans in the temperature range from 25 to

600 °C with a heating rate of 10 °C min^{-1}. Unless otherwise noted, a sample mass of ca. 8 mg was employed. Samples featuring Pt-complexes were measured with a heating rate of 1 °C min^{-1}.

X-Ray Scattering. Small angle X-ray scattering (SAXS) was performed with a NanoMax-IQ camera (Rigaku Innovative Technologies, Auburn Hills, MI, USA). The camera was equipped with a Cu target sealed tube source (MicroMax 003 microfocus, Rigaku) and the scattering data were recorded by a Pilatus 100 K detector (Dectris). The radii of the nanoparticles (R_P) were obtained by adapting a polydisperse spherical model to the form factor of the SAXS profiles. The values obtained are from individual measurements ± standard deviation (σ) are given and the standard deviation was obtained from $\sigma = R_p \times$ PDI, where PDI stands for the polydispersity index value applied to the model.

Derivation of Particle Distances. The derivation of theoretical values d_{nn}^{pred} for the distribution of particles in the nanocomposites was carried out by assuming that all platinum atoms were converted into spherical particles with non-disperse radius R_P and homogeneously distributed within the polymer matrix. The value of d_{nn}^{pred} can then be estimated from

$$d_{nn}^{pred} = \left(\frac{3V_S}{4\pi N_P}\right)^{\frac{1}{3}}, \quad (1)$$

with V_s as the sample volume, and N_p as the total number of particles. The latter is given by

$$N_P = \frac{3\phi_P V_S}{4\pi {R_P}^3}. \quad (2)$$

The term φ_P represents the particles volume fraction in the sample and can be calculated from the particles mass fraction W_p, the particle density ρ_P, and the density of the polymer matrix ρ_M. The particle density and the density of the polymer matrix are assumed to be equivalent to the density values $\rho_{Pt} = 21.45$ g cm^{-3} for Platinum and a density of $\rho = 1.00$ g cm^{-3} was assumed for the organic polymer matrix. The mass fraction was calculated based on the macromonomer molecular weight and the metal stoichiometry.

$$\phi_P = \frac{\rho_M W_P}{\rho_M W_P + (1 - W_P)\rho_P}. \quad (3)$$

Combining (1) and (2) yields:

$$d_{nn}^{pred} = \frac{R_P}{\phi_P^{1/3}} \quad (4)$$

from which the desired values for the theoretical average nearest neighbor distances were determined.

Optical Microscopy. Optical microscopy images were acquired with an Olympus BX51 microscope equipped with a DP72 digital camera.

Mechanical Characterization. Tensile tests were performed in a TA Instruments DMA Q 800 at 25 °C with a strain rate of 5 % min^{-1} using dog-bone shaped samples of the following approximate dimensions: 15 × 3 × 0.2 mm (length/width/thickness). Data are reported as averages of 3 independent measurements. The

provided Young's moduli were calculated from the slope in the linear region of the stress strain curve (tangent modulus at a stress of 0.025 MPa).

Transmission Electron Microscopy. Samples for scanning transition electron microscopy (STEM) were prepared by microtomy of bulk **N1**–**N3** samples. High-angle annular dark-field (HAADF) STEM images and EDX spectra were acquired using an aberration-corrected (double Cs-corrected) Thermo Scientific Titan Themis 60-300, equipped with a high brightness Schottky X-FEG gun, a Super-X EDX system comprising four silicon drift detectors, and Velox acquisition software. Unless otherwise noted, HAADF-STEM images and EDXS data were acquired with an acceleration voltage of 200 kV and beam currents of 150 pA and 500 pA, respectively.

Particle Size Analysis. The analysis of transmission electron microscopy images for the size distribution of Pt-nanoparticle sizes was performed with the Fiji distribution of the ImageJ image processing software. The contrast and brightness of the TEM micrographs was adjusted, and the background was subtracted. The images were subsequently subjected to a classification and segmentation by a threshold analysis with the *Trainable Weka Segmentation* plugin. The Pt-nanoparticles were manually defined and separated in repeated segmentation steps with straight and free-hand lines from the background. The resulting images were then converted into 8-bit files, an area threshold was applied (0.25 – 30 nm^2; circularity of 0.85–1), and the size distribution of the particles was determined. Aggregates of nanoparticles and superimposed nanoparticles were not taken in account. The mean interparticle distances and sizes were obtained by calculating the average values over sets of >100 individual measurements.

Catalysis Measurements. The gas volume formed during the catalytic reactions of hydrogen peroxide and ammonia borane were determined by volumetric measurements (as previously reported, see Figure S29 for a detailed schematic of the setup).[2] For the oxygen evolution by decomposition of hydrogen peroxide, a solution of hydrogen peroxide (7.3 M) in aqueous ethyl acetate was placed in a 50 mL round bottom flask together with the sample of the nanocomposite. A closed 100 mL pressure-equalizing dropping funnel filled with 100 mL of water was placed over the 50 mL round bottom flask containing 50 mL of a 1 M H_2O_2 aqueous ethyl acetate solution and the setup was closed with a septum. An empty 100 mL graduated cylinder was placed higher than the pressure-equalizing dropping funnel and connected via a stainless-steel cannula. The cannula was completely submerged in the water and the difference in height between both the dropping funnel and the graduated cylinder was set to 18 cm. The overpressure of formed oxygen gas led to the displacement of water through a stainless-steel cannula into a graduated cylinder. The amount of displaced water was measured over time to determine the rate of oxygen formation for the different nanocomposite samples **N1–N3** (ca. 1–3 mg; 200 °C, 1 h). The same procedure was followed with either an aqueous hydrogen peroxide (7.3 M) solution or an ammonia borane (0.5 M) solution in water to determine the respective catalytic activity of the nanocomposites.

4. Chemical Syntheses and Materials Preparation

Materials and General Procedures. Unless otherwise noted, all reactions were carried out in dried Schlenk glassware in an inert nitrogen atmosphere. Dichloromethane (DCM), ethyl acetate, hexane, diethyl ether, and methanol were purchased as analytical grade from either Sigma-Aldrich, Honeywell, or Fluka and were used without further purification. Anhydrous dimethyl formamide (DMF) and toluene were purchased from Sigma-Aldrich. 4-Iodophenol (99%, Aldrich), phenylacetylene (98%, Aldrich), pyridine (ACS reagent, ≥99.0%, Sigma-Aldrich), potassium carbonate (99.995%, Aldrich), hydrochloric acid (ACS reagent, 37%, Sigma-Aldrich) triphenylphosphine (99% ReagentPlusR, Sigma-Aldrich), copper(I) iodide (98%, Sigma-Aldrich) bis(triphenylphosphine) palladium(II) dichloride (98%, Sigma-Aldrich), platinum(II) chloride (99.9 %, Aldrich), *p*-toluenesulfonyl chloride (≥98%, Sigma Aldrich), hydroxyl terminated poly(tetrahydrofuran) of a number-average molecular weight (M_n) of 1000, 2000, 2900 g mol^{-1} (99%, Sigma Aldrich) were used as received. Styrene (99.9%, Aldrich) was distilled once prior to use. Triethylamine (≥99.5%, Aldrich) was dried over CaH_2 and distilled once prior to use. 4-Phenylethylene phenol was synthesized following a procedure adapted from the literature.[3] A styrene solution of $Pt^0(styrene)_3$ (2.19×10^{-2} M) was prepared following a reported procedure.[4,5] Thin layer chromatography (TLC) was performed on TLC plates from Merck (Silica gel 60 F254). UV-light (254 or 365 nm) or potassium permanganate were used for detection. Column chromatography was conducted on Geduran silica gel Si 60 from Merck (40–60 μm).

Protocol for the Preparation of the Metallosupramolecular Polymers P1–P3. Macromonomer **1** (ca. 75.16 mg, 39.6 μmol) was added to a vial, dissolved in a $Pt^0(styrene)_3$ solution (2.79 mL, 39.6 mmol, $c(Pt(sty)_3)$ = 0.014 mol L^{-1}), and the solution was stirred for 1 h to ensure successful ligand exchange. All concentrations were determined by spectrophotometric titrations prior to use (*vide supra*). After stirring, the mixture was cast onto a polytetrafluoroethylene (PTFE) substrate and dried under vacuum for 24 h. After drying, a sample of the tacky film of **P1** was redissolved in $CDCl_3$ and the complete ligand exchange was confirmed by ^{1}H-NMR spectroscopy. The preparation of the MSPs **P2** and **P3** followed the same procedure.

Protocol for the Preparation of the Nanocomposites N1–N3. Unless otherwise noted, solvent cast samples of **P1**–**P3** were subjected to heating at temperatures above 120 °C to induce the formation of the nanocomposites **N1**–**N3**. To prepare films of the nanocomposite with a uniform thickness, samples of P1–P3 were subjected to compression molding samples in between PTFE sheets in a Carver CE Press at 120 °C for 1 h with a pressure of 3 tons. Heating at higher temperatures was carried out in a Binder vacuum oven under an inert nitrogen atmosphere. To induce the formation of the nanocomposite by UV irradiation, solvent-cast samples of **P1**–**P3** on quartz glass slides or PTFE sheets were irradiated with a UV probe (Ocean Optics, 320–390 nm) through a custom-made cardboard mask or a quartz-chromium photomask. Alternatively, a laser engraving machine (INSMA) was used to induce the nanocomposite formation from such samples upon microlaser irradiation (400–460 nm, 4000 mW).

Protocol for Spin Coating and Sample Processing for TEM Measurements. An exemplary protocol for the processing is provided based on the processing of macromonomer **1**, which was used in the same way for macromonomers **2** and **3**. The macromonomer **1** (8.01 mg, 4.22 µmol) was added to a vial, dissolved in a $Pt^0(styrene)_3$ solution (0.295 mL, 4.13 µmol, $c(Pt(Sty)_3)$ = 0.014 mol L^{-1}) solution, and the mixture was stirred for 1 h to ensure complete ligand exchange reaction. All concentrations were determined by spectrophotometric titrations prior to use (*vide supra*). For spin coating, a TEM grid was placed on a microscopy glass slide substrate on the spin coater (Spin coater Model P6700, Specialty Coating Systems, Inc.) and 3 µL of the solution of **P1** was deposited with a micropipette. The TEM grid was then spun using the following program:

1. 200 rpm for 15 s,

2. 2000 rpm for 15 s,

3. 3100 rpm for 1 s.

This protocol was used for the deposition of samples on quartz slide or TEM grids. The prepared thin spin-coated films were subsequently heated to different temperatures in a vacuum oven (Binder) under an inert nitrogen atmosphere.

Synthesis of telechelic bis(*p*-toluenesulfonyl ester)-functionalized poly(tetrahydrofuran).

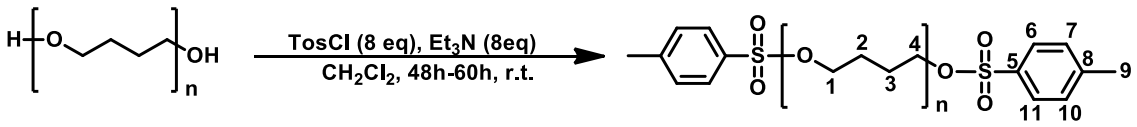

PTHF M_n 1000 g mol^{-1}: The preparation of bis(*p*-toluenesulfonyl ester)-functionalized poly(tetrahydrofuran) was carried out according to a previously reported procedure.[2] Hydroxyl terminated poly(tetrahydrofuran) (M_n: 1000 g mol^{-1}, 2.0 g, 1.98 mmol, 1.0 eq.) was placed in a previously dried round-bottom flask equipped with a stir bar. $CHCl_3$ (30 mL) was added, and the mixture was stirred at room temperature until a colorless solution was obtained. *p*-Toluenesulfonyl chloride (3.05 g, 15.84 mmol, 8.0 eq.) was added and the solution was cooled to 0 °C. Triethylamine (1.93 mL, 13.86 mmol, 7.0 eq) was added dropwise and the solution was stirred for 48 h at room temperature. Ethyl acetate (40 mL) was added, and the organic phase was washed with HCl (aq., 0.01%) until neutral pH was reached. The organic phase was washed once with saturated NaCl solution, dried over $MgSO_4$, filtered, and the solvent was removed *in vacuo*. The obtained yellow oil was then passed over a plug of silica gel (< 2 cm height, hexane/chloroform 10:1 to ethyl acetate/methanol 9:1) to yield telechelic bis(*p*-toluenesulfonyl ester)-functionalized poly(tetrahydrofuran) (1.75 g, mmol, 88 %).

^{1}H NMR (400 MHz, $CDCl_3$): δ = 7.77 (d, *J* = 8.3 Hz, C$H^{6,11}$, 4H), 7.33 (d, *J* = 8.0 Hz, C$H^{7,10}$, 4H), 4.04 (t, *J* = 6.8 Hz, –O–CH_2–, 4H), 3.40 (m, C$H^{1,4}$, 75H), 2.44 (s, CH_3^9, 6H), 1.77 (m, $CH_2^{2,3}$ 82H).

PTHF M_n 2000 g mol^{-1}: The preparation followed the above-described procedure using hydroxyl terminated poly(tetrahydrofuran) (M_n: 2000 g mol^{-1}, 3.0 g, 1.5 mmol) in $CHCl_3$ (30 mL) with *p*-toluenesulfonyl chloride

(2.28 g, 12 mmol, 8.0 eq.) and triethylamine (1.46 mL, 10.5 mmol, 7.0 eq.) The oil obtained after aqueous workup was passed over a plug of silica gel (< 2 cm height, hexane/chloroform 10:1 to ethyl acetate/methanol 9:1) to yield telechelic bis(*p*-toluenesulfonyl ester)-functionalized poly(tetrahydrofuran) (2.48 g, mmol, 84 %).

^{1}H NMR (400 MHz, $CDCl_3$): δ = 7.78 (d, J = 8.3 Hz, C$H^{6,11}$, 4H), 7.33 (d, J = 8.0 Hz, C$H^{7,10}$, 4H), 4.04 (t, J = 12.9 Hz, –O–CH_2–, 4H), 3.40 (m, C$H^{1,4}$, 130H), 2.44 (s, CH_3^9, 6H), 1.59 (m, $CH_2^{2,3}$, 137H).

PTHF M_n 2900 g mol^{-1}: The preparation followed the above-described procedure using hydroxyl terminated poly(tetrahydrofuran) (M_n: 2900 g mol^{-1}, 3.0 g, 1.5 mmol) in $CHCl_3$ (30 mL) with *p*-toluenesulfonyl chloride (1.58 g, 8.0 mmol, 8.0 eq.) and triethylamine (1.0 mL, 7.17 mmol, 7.0 eq.) The oil obtained after aqueous workup was passed over a plug of silica gel (< 2 cm height, hexane/chloroform 10:1 to ethyl acetate/methanol 9:1) to yield telechelic bis(*p*-toluenesulfonyl ester)-functionalized poly(tetrahydrofuran) (2.60 g, mmol, 88 %).

^{1}H NMR (400 MHz, $CDCl_3$): δ = 7.78 (d, J = 8.2 Hz, C$H^{6,11}$, 4H), 7.33 (d, J = 8.1 Hz, C$H^{7,10}$, 4H), 4.04 (t, J = 6.4 Hz, –O–CH_2–, 4H), 3.40 (m, C$H^{1,4}$, 186H), 2.44 (s, CH_3^9, 6H), 1.61 (m, $CH_2^{2,3}$, 201H).

Synthesis of bis-diphenylacetylene terminated poly(tetrahydrofuran) macromonomers 1–3.

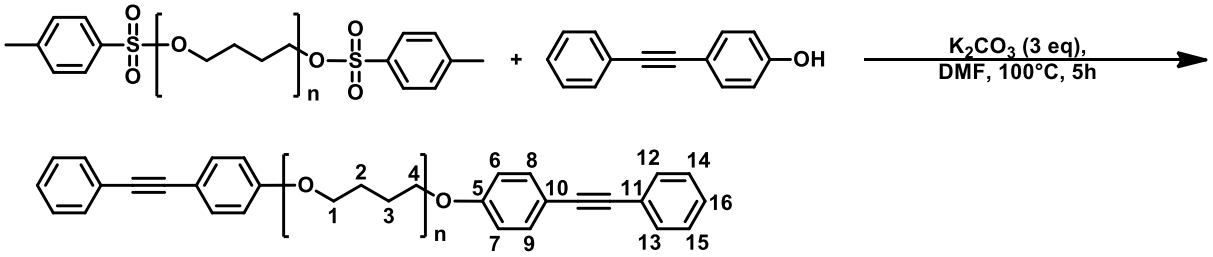

Macromonomer **1**: Tosylated poly(tetrahydrofuran) (M_n: 1156 g mol^{-1}, 1.0 g, 0.8 mmol, 1 eq.), 4-(phenylethynyl)phenol (0.509 g, 2.5 mmol, 3 eq.), and potassium carbonate (0.355 g, 2.5 mmol, 3 eq.) were added to a round-bottom flask. After degassing in vacuo for 10 min, the mixture was placed under a nitrogen atmosphere, anhydrous DMF (12 mL) was added, and the stirred mixture was heated to 105 °C for 5 h. Ethyl acetate (100 mL) was added, the mixture was washed twice with saturated NaCl solution, dried over Na_2SO_4, and the solvent was removed in vacuo. The oily residue was passed over a plug of silica gel (< 2 cm height, chloroform/hexane 2:1 to ethyl acetate). The solvent was removed in vacuo and **1** was obtained as a tan oil (0.91 g, 0.59 mmol, 68%).

^{1}H NMR (400 MHz, $CDCl_3$): δ = 7.60 (d, J = 8.0 Hz, C$H^{13,12}$, 2H), 7.54 (d, J= 8.9 Hz,C$H^{14,15}$, 4H), 7.42 (d, J = 7.3 Hz, C$H^{8,9,16}$, 6H), 6.95 (d, J = 8.8 Hz, C$H^{6,7}$, 4H), 4.09 (t, J = 6.4 Hz, –O–CH_2–, 4H), 3.53 (m, $CH_2^{1,4}$, 76H), 2.02–1.58 (m, $CH_2^{2,3}$, 85H). MS (MALDI): calcd. for $C_{84}H_{130}O_{15}Ag$ ([M(n = 14)+Ag]$^+$) 1487.82; found 1437.11.

Macromonomer **2**: The preparation followed the above-described procedure using tosylated poly(tetrahydrofuran) (M_n: 2156 g mol^{-1}, 1 g, 0.5 mmol, 1 eq.), 4-(phenylethynyl)phenol (0.509 g, 1.4 mmol, 3 eq.), and potassium carbonate (0.190 g, 1.4 mmol, 3 eq.). The oily residue obtained after the reaction and aqueous

workup was passed over a plug of silica gel (< 2 cm height, chloroform/hexane 5:1 to ethyl acetate/methanol 9:1). The solvent was removed in vacuo and **2** was obtained as a tan oil (0.84 g, 0.33 mmol, 72%).

^{1}H NMR (400 MHz, $CDCl_3$): δ = 7.50 (d, J = 8.0 Hz, $CH^{13,12}$, 4H), 7.45 (d, J = 8.8 Hz, $CH^{14,15}$, 4H), 7.32 (d, J = 7.3 Hz, $CH^{8,9,16}$, 6H), 6.86 (d, J = 8.8 Hz, $CH^{6,7}$, 4H), 4.00 (t, J = 6.4 Hz, –O–CH_2–, 4H), 3.41 (m, $CH_2^{1,4}$, 133H), 1.61 (m, $CH_2^{2,3}$, 141H). MS (MALDI): calcd. for $C_{140}H_{242}O_{29}Ag$ ([M(n = 28)+Ag]$^+$) 2497.32; found 2205.19.

Macromonomer **3**: The preparation followed the above-described procedure using tosylated poly(tetrahydrofuran) (M_n: 3056 g mol^{-1}, 1.0 g, 0.3 mmol, 1 eq.), 4-(phenylethynyl)phenol (0.193 g, 1.0 mmol, 3 eq.), and potassium carbonate (0.134 g, 1.0 mmol, 3 eq.). The oily residue obtained after the reaction and aqueous workup was passed over a plug of silica gel (< 2 cm height, chloroform/hexane 5:1 to ethyl acetate/methanol 9:1). The solvent was removed in vacuo and **3** was obtained as a yellow oil (0.77 g, 0.22 mmol, 69%).

^{1}H NMR (400 MHz, $CDCl_3$) δ = 7.50 (d, J = 7.8, 1.7 Hz, $CH^{13,12}$, 4H), 7.45 (d, J = 8.9 Hz, $CH^{14,15}$, 4H), 7.32 (d, J = 7.3 Hz, $CH^{8,9,16}$, 6H), 6.86 (d, J = 8.9 Hz, $CH^{6,7}$, 4H), 4.00 (t, J = 6.4 Hz, –O–CH_2–, 4H), 3.41 (m, $CH_2^{1,4}$, 168H), 1.62 (m, $CH_2^{2,3}$, 189H). MS (MALDI): calcd. for $C_{196}H_{354}O_{43}Ag$ ([M(n = 40)+Ag]$^+$) 3506.82.2; found 1995.82.

Synthesis of 4-(phenylethynyl)phenol.

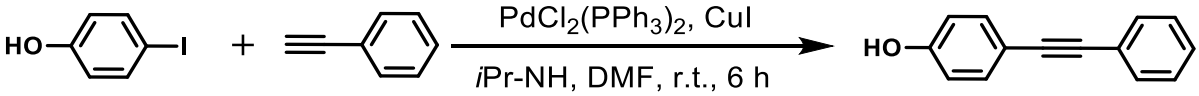

4-Iodophenol (2.0 g, 9.1 mmol, 1 eq.) and phenylacetylene (2.32 g, 22.7 mmol, 2.5 eq.) were added to anhydrous DMF (13 mL) and distilled triethylamine (26 mL), triphenyl phosphine (119 mg, 0.045 mmol, 0.05 eq.), and $PdCl_2(PPh_3)_2$ (319 mg, 0.045 mmol, 0.05 eq.) were consecutively added. The reaction mixture was purged with a flow of nitrogen for 30 min, copper(I) iodide (86 mg, 0.045 mmol, 0.1 eq.) was added, the mixture was again purged with nitrogen for 10 min, and left stirring at room temperature for 6 h. The mixture was adjusted to pH 2 by addition of 2 M HCl and subsequently extracted three times with ethyl acetate (40 mL). The combined organic layers were washed once with saturated NaCl solution, dried over Na_2SO_4, and the solvent was removed *in vacuo*. Purification by column chromatography (silica gel, hexane/ethyl acetate 10:1) afforded 4-(phenylethynyl)phenol (2 g, 7.2 mmol, 80%) as a nacre/yellow solid.

^{1}H NMR (400 MHz, $CDCl_3$): δ = 7.51 (d, J = 7.8 Hz, C*H5*,6, 2H), 7.43 (d, J = 8.5 Hz, C*H*3,4, 2H), 7.37–7.28 (m, C*H*7-9, 3H), 6.81 (d, J = 8.5 Hz, C*H*1,2, 2H), 4.99 (s, OH, 1H).

5. NMR Spectra

^{1}H NMR spectrum ($CDCl_3$, 400 MHz) of tosylated poly(tetrahydrofuran) (M_n(PTHF): 1000 g mol^{-1}).

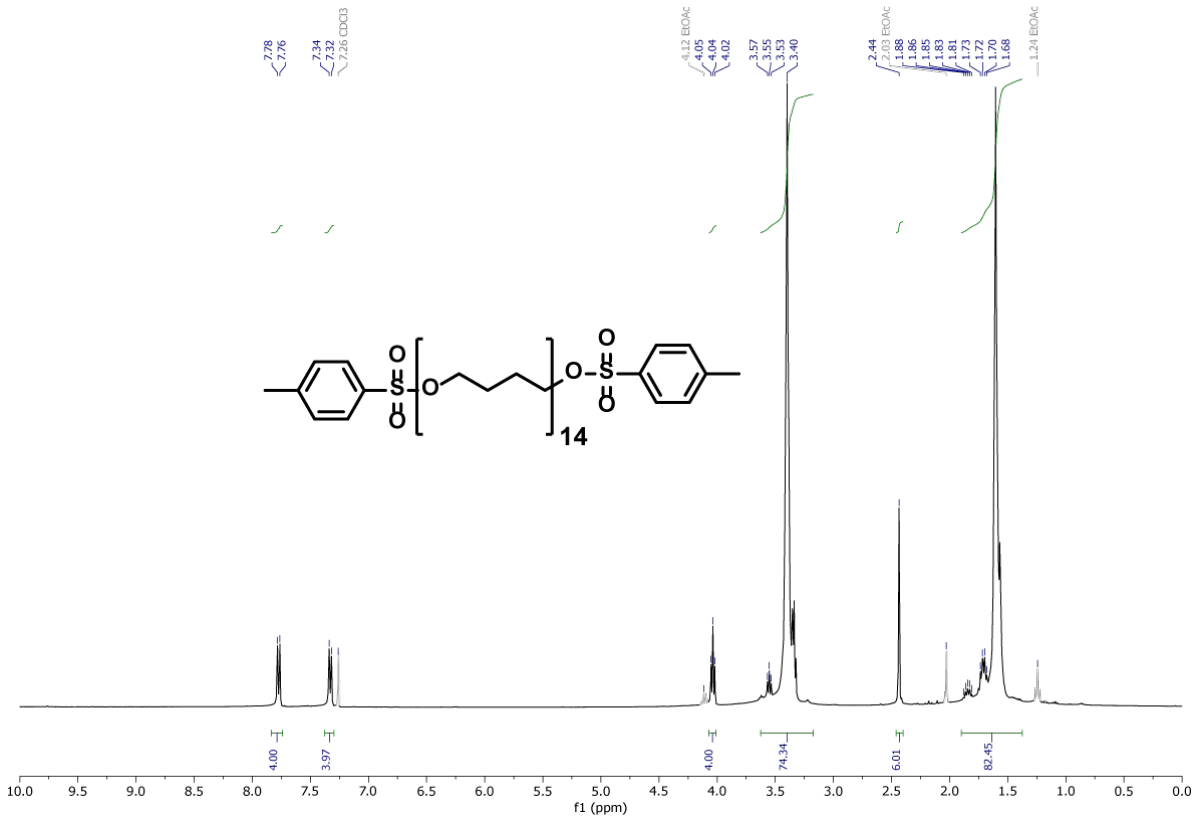

^{1}H NMR spectrum ($CDCl_3$, 400 MHz) of tosylated poly(tetrahydrofuran) (M_n(PTHF): 2000 g mol^{-1}).

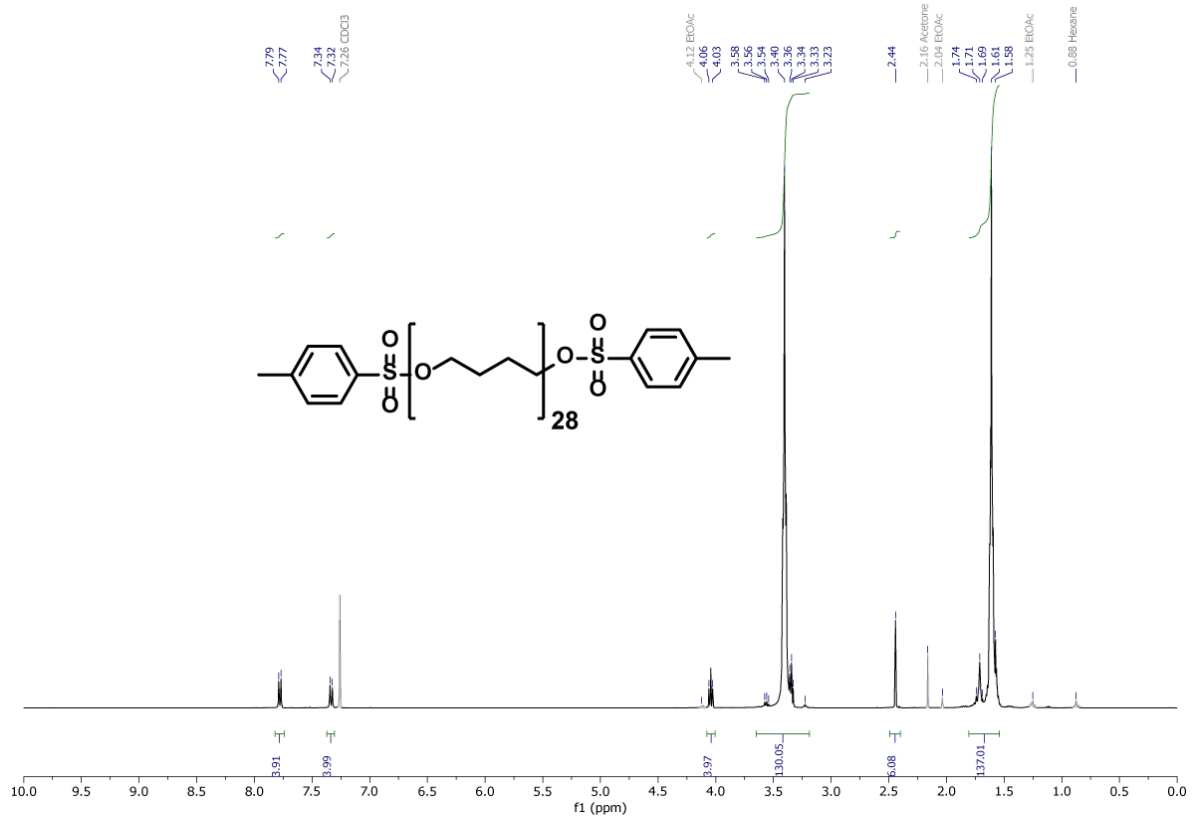

^{1}H NMR spectrum ($CDCl_3$, 400 MHz) of tosylated poly(tetrahydrofuran) (M_n(PTHF): 2900 g mol^{-1}).

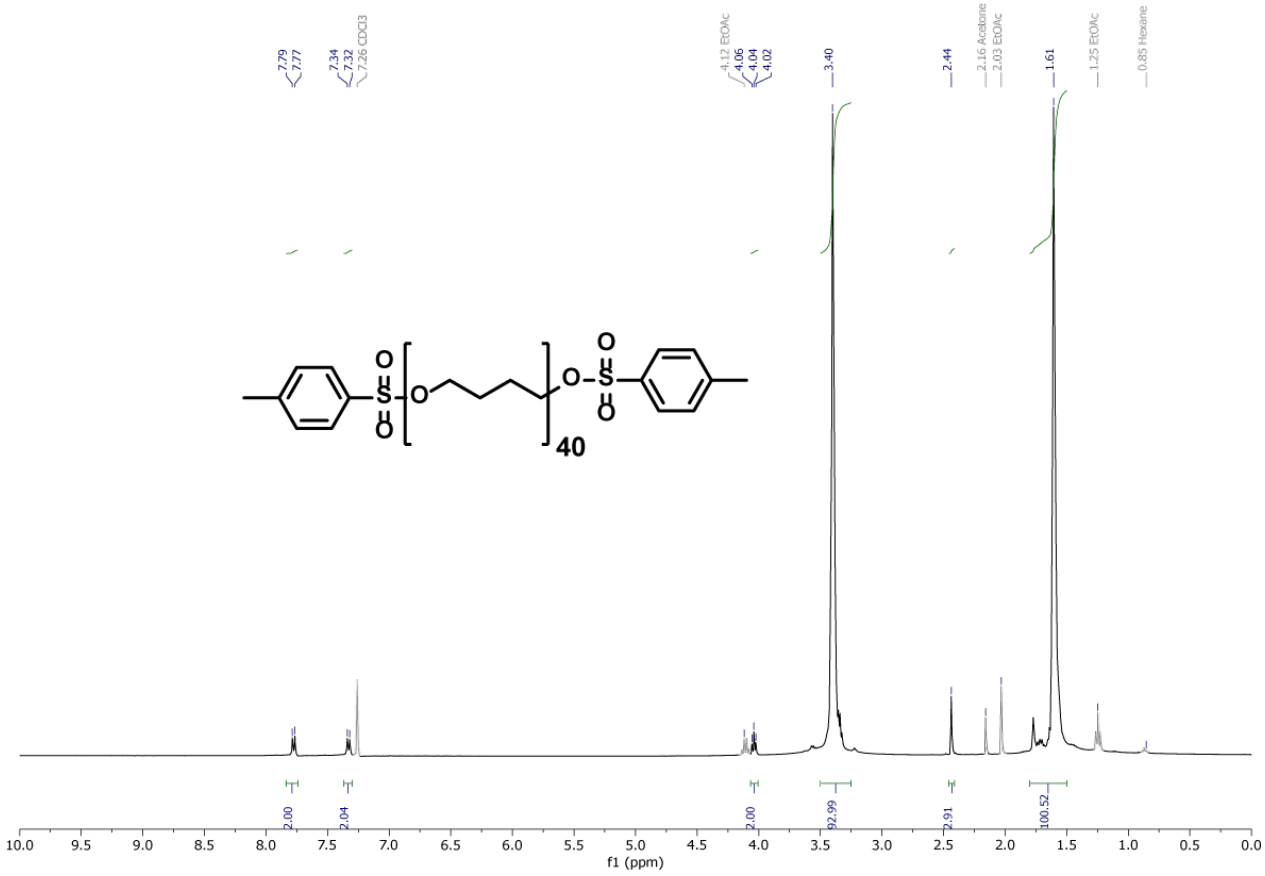

^{1}H NMR spectrum ($CDCl_3$, 400 MHz) of macromonomer **1**.

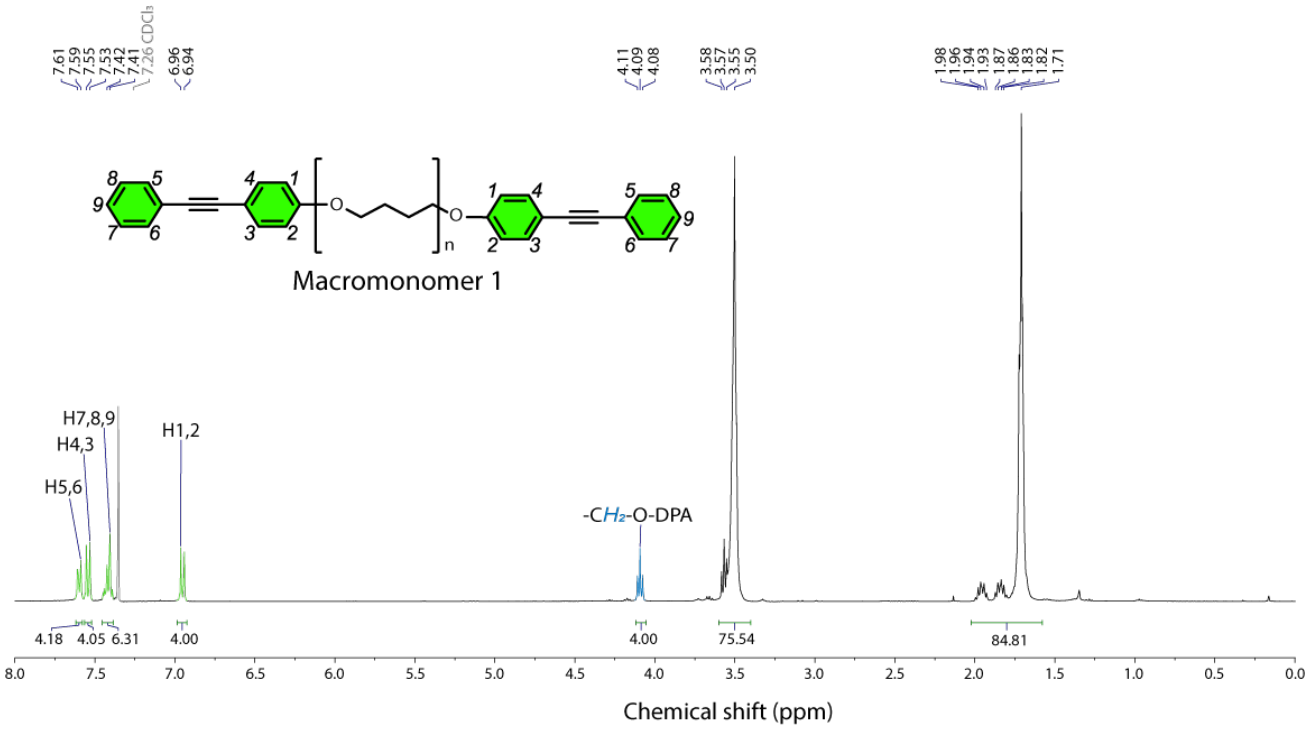

^{1}H NMR spectrum ($CDCl_3$, 400 MHz) of macromonomer **2**.

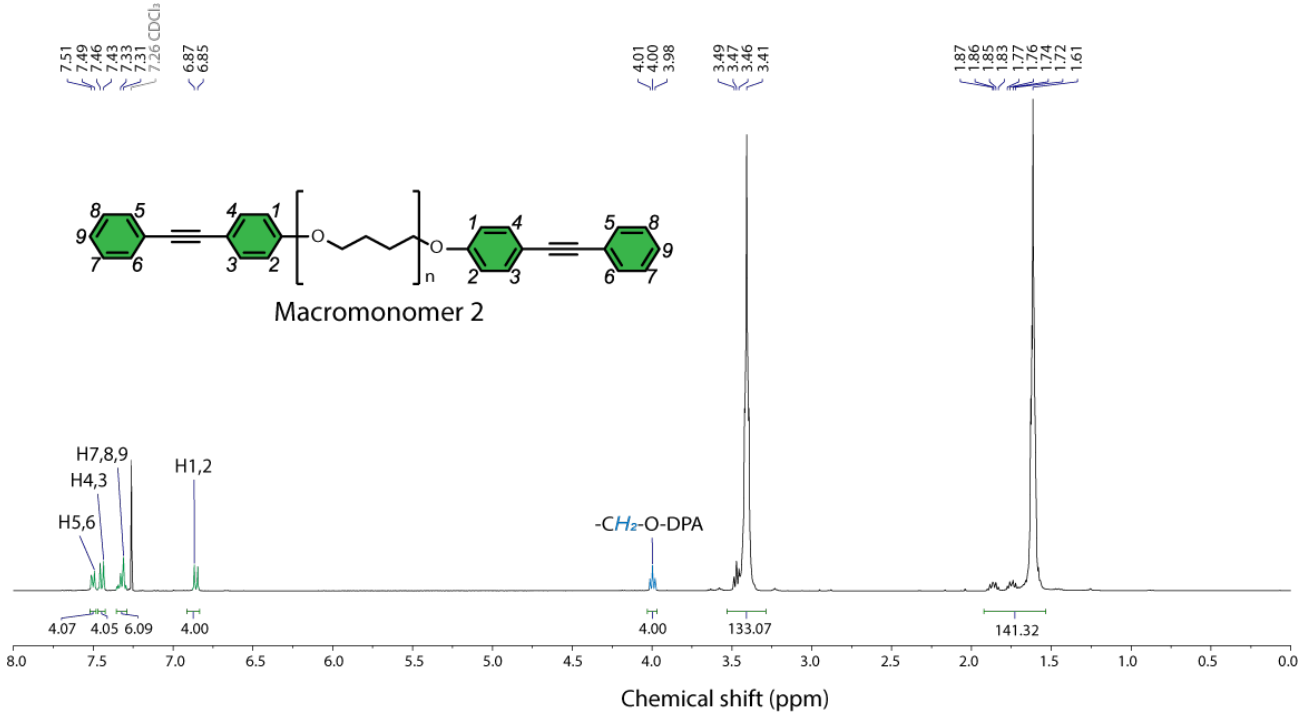

^{1}H NMR spectrum ($CDCl_3$, 400 MHz) of macromonomer **3**.

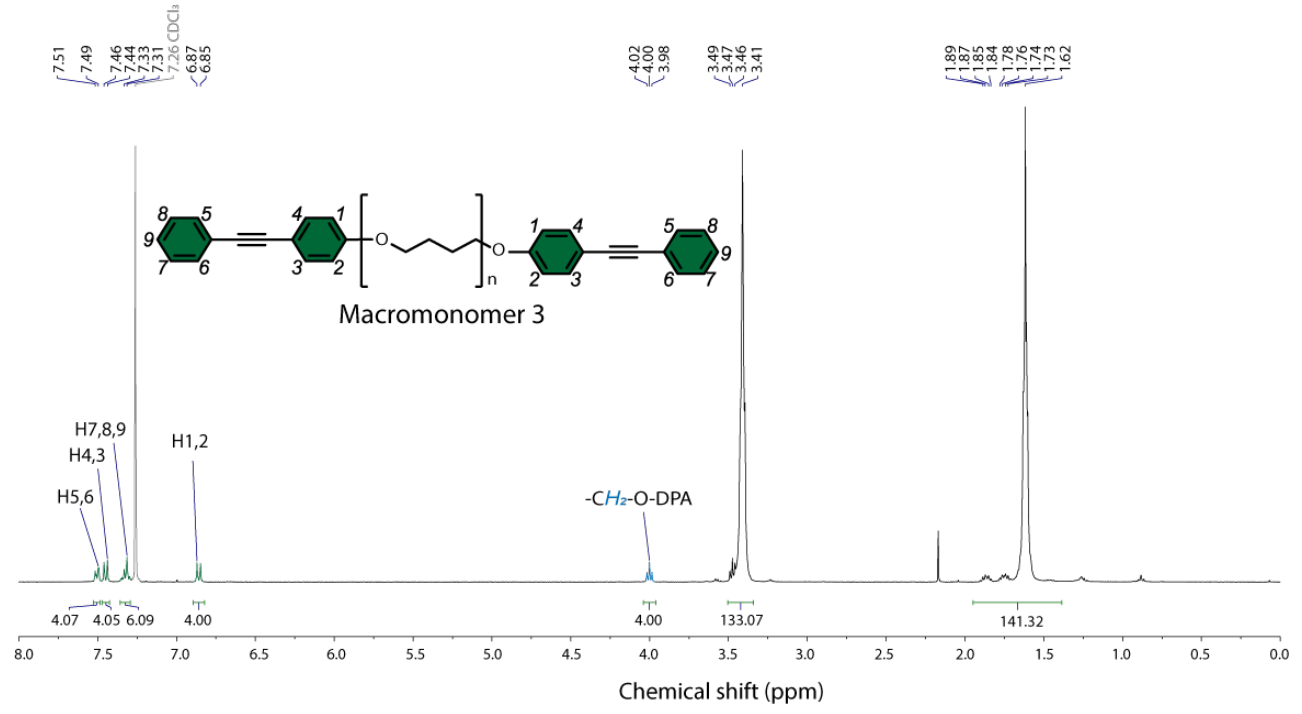

^{1}H NMR spectrum ($CDCl_3$, 400 MHz) of 4-phenylethynyl-phenol.

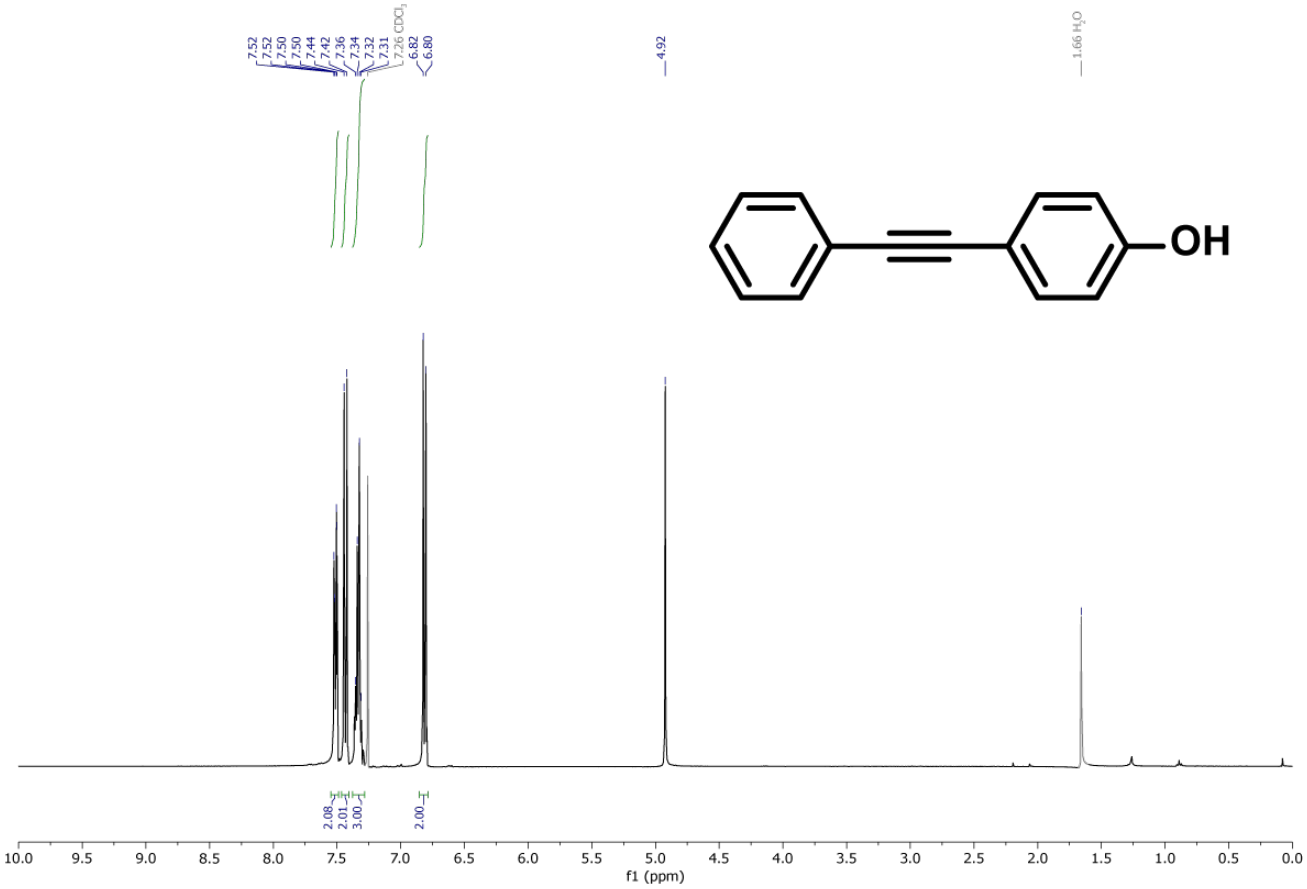

6. References

1 A. Fournet and G. Guinier, *Small-Angle Scattering of X-Rays*, John Wiley & Sons, Inc., New York, 1955.

2 L. M. Olaechea, L. Montero de Espinosa, E. Oveisi, S. Balog, P. Sutton, S. Schrettl and C. Weder, *J. Am. Chem. Soc.*, 2020, **142**, 342–348.

3 C. K. W. Jim, J. W. Y. Lam, C. W. T. Leung, A. Qin, F. Mahtab and B. Z. Tang, *Macromolecules*, 2011, **44**, 2427–2437.

4 W. Caseri and P. S. Pregosin, *Organometallics*, 1988, **7**, 1373–1380.

5 A. Albinati, W. R. Caseri and P. S. Pregosin, *Organometallics*, 1987, **6**, 788–793.